Chapter 2: Hydro-geomorphic characterization of Manas-Beki river basin

2.1 Introduction

Hydrogeomorphic characterization is the quantitative description of a drainage basin which can be correlated to the hydrologic response of a basin [1]. Fluvial processes and channel planform develop gradually through time adjusting themselves towards self-stabilization [2]. River systems are highly sensitive to changes in the hydrological regime altering the geomorphic processes and leading consequently to geomorphic hazards, particularly in areas of high energy environment such as the Manas-Beki river basin [3, 4, 5]. Analysis of the basin morphometric parameters and fluvial dynamics can be effective knowledge base to understand geomorphic responses to natural and anthropogenic changes [6, 7]. The scope of this chapter includes the following aspects of the Manas-Beki river basin:

i. Morphometric analysis of the Manas-Beki river basin including the basin form, linear, areal, and relief aspects.
ii. Analysis of channel and planform changes in the floodplain stretch of the Manas-Beki river from 1990 to 2020. This includes:
    a. Changes in sinuosity and braiding intensity
    b. Channel change analysis
    c. Spatial variations in erosion and deposition due to channel shifts

Morphometric analysis is the measurable description of a drainage basin and can be grouped into linear aspects of the channel network, areal aspects of the drainage basin, relief aspects of the channel system, and basin form [8]. Morphometric analysis has been widely used to understand landscape development and relations between landforms and processes [9, 10, 11]. Morphometric parameters of a river basin give an understanding of how the basin responds to changes in streamflow and is crucial information for hazard analysis especially floods and landslides [1, 12-14]. Drainage basin morphometry is vital information to understand the hydro-geomorphic response of the drainage basin to changes in the climate [15-19] and the use of satellite images, DEM, and Geographical Information System (GIS) has proved to be the easiest and most reliable method for faster and more accurate quantitative estimation of drainage basin parameters widely used over the years by researchers worldwide [20-27].

Rivers change frequently with respect to the streamflow and sediment flow owing to changes in the environment either naturally or due to anthropogenic causes [2]. These changes are evident through changes in the spatial representation of the channel [28]. Channel changes may

occur in various ways like alteration of the direction of flow due to neck cut-off, widening of the channel in response to bar development, development of anabranches as well as progressive shifting of meander bends [29]. Analysis of channel changes has been undertaken by many researchers over the last few decades, especially with the use of RS and GIS techniques [30-38]. Channel dynamics studies have been primarily executed to support solving the issues related to river management and riverine hazards such as floods and erosion in the downstream regions where the topography is relatively flat, and rivers interact with the human environment [39-45]. The Himalayan rivers are observed to be changing rapidly over the years largely attributed to the changes in sediment flow [46] and observed changes in climate coupled with human interferences of the natural environment [47-52].

Apart from morphometric parameters, analysis of channel morphology and planform changes are crucial to understand the hydro-geomorphic implications of climate change. Analysis of the channel dynamics of the tributaries of the Brahmaputra river revealed the entire basin as an active zone for fluvial processes and further studies to examine the changes more closely for individual tributaries were suggested [46, 53]. This objective aims to develop the effective baseline information for the Manas-Beki river basin including the basin morphometry and morphological changes of the channel in the floodplains.

2.2 Data and Methods

2.2.1 Data and resources used

Morphometric analysis and analysis of channel planform changes were carried out using RS and GIS techniques. Satellite data processing and digital analyses were carried out using the ERDAS Imagine software and all geospatial analyses were carried out using ArcGIS software. Various geospatial data were used as required for carrying out the research work, the details of which is presented in Table 2.1. For morphometric analysis, Survey of India (SOI) topographical maps and Landsat satellite images of 30 m spatial resolution obtained from NASA's Earth Explorer data portal, were utilized along with Shuttle Radar Topography Mission (SRTM) DEM of 30 m spatial resolution obtained from United States Geological Survey (USGS). To ensure the recent structure of the streams and identify smaller streams, high-resolution LISS-IV (Linear Imaging Self Scanning Sensor) satellite images of 5.6 m spatial resolution for the study area procured from National Remote Sensing Centre (NRSC) were utilized.

Table 2.1 Details of data used for hydrogeomorphic characterization of Manas-Beki river basin

Dataset	**Resolution/ scale**	**Sources**	**Year**
Topographical maps	1:50000	SOI	Surveyed between 1958-89
LISS IV images	5.8 m	NRSC	2016
SRTM DEM	30 m	USGS	2015
Landsat images	30 m	NASA	1990, 2000, 2010, 2020
Sentinel-2 images	10 m	ESA	2020

For analyzing the channel changes, Landsat satellite images of four different periods were used: 1990, 2000, 2010, and 2020. Images were selected for the months of November or December for all the years to maintain the same season data over the years as cloud-free images are only found over the study area after the monsoon season which extends from the months of June to October.

2.2.2 Methodology

The overall methodology used for hydrogeomorphic characterization of the Manas-Beki river basin is given in Figure 2.1. Geospatial analytics and tools were used to accomplish the outcomes of the first objective. The detailed methods used for specific analyses are outlined in the following sub-sections.

Morphometric analysis

Drainage basin boundaries and identification of streams within the basin are required for the morphometric analysis. The streams in the hilly upper catchment were extracted from the SRTM DEM in a GIS environment. Delineation of streams in the almost flat floodplain areas was completed using SOI topographical maps and to ensure the recent structure, high-resolution LISS-IV satellite data was used, as the tributaries of Brahmaputra change their courses in the plains very frequently. Some of the complex interconnecting streams were simplified as a compulsion to meet the current stream classification methods. The drainage basin boundary was delineated with the help of contours and ends of the identified streams. Basic parameters of basin form including basin area, perimeter, basin length, minimum and maximum basin height were calculated using GIS software from the delineated basin and stream boundaries and elevation information from DEM.

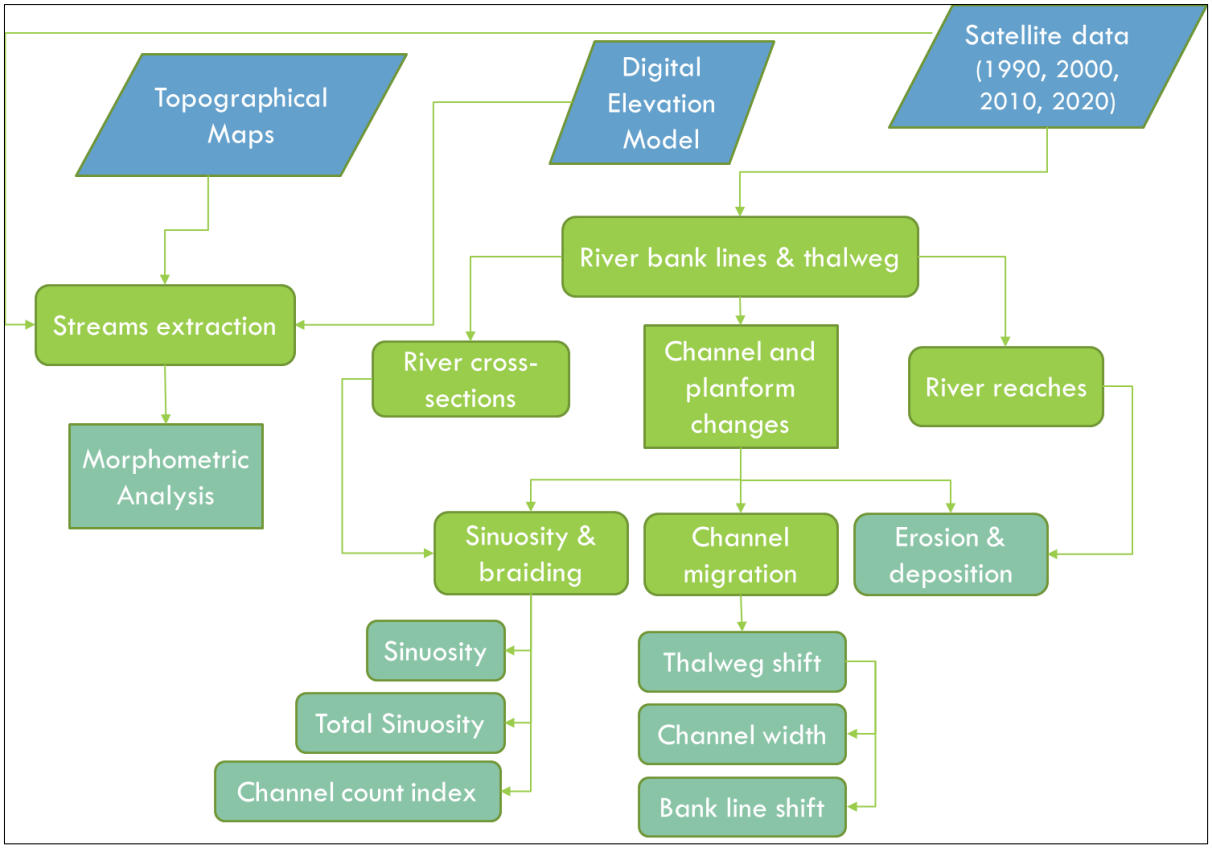

Figure 2.1 The schema of methodology used for hydrogeomorphic characterization of Manas-Beki river basin

The morphometric parameters including the measurements related to the linear, areal, and relief aspects of the basin were calculated using established mathematical expressions. The parameters included in this study and the expressions used for estimating the parameters are presented in Table 2.2.

Table 2.2 Morphometric parameters and their mathematical expressions

Morphometric Parameters	**Methodologies**	**Source**	Where, Lu = Total stream length of order u Nu = Total number of streams of order u Nu+1= Total number of stream of next higher order ALu = Average length of streams of order u
Linear aspects			
Stream order	---	Strahler; Sah and Das [54, 55]	
Stream length (Lu)	---	Horton [56]	
Mean stream length (Lsm)	Lsm = Lu/ Nu	Strahler [54]	
Stream length ratio (Rl)	Rl= ALu/ALu-1	Horton [56]	
Bifurcation ratio (Rb)	Rb = Nu/ Nu+1	Horton [8]	
Rho co-efficient (ρ)	RHO = Rl/Rb	Horton [56]	
Areal aspects			

Drainage density (Dd)	Dd = L/A	Horton [56]	ALu-1 = Average length of streams of next lower order L = Total length of streams A = Area of basin N = Total number of streams P = Perimeter of basin Lb = basin Length H = Highest basin height h = Lowest basin height
Stream frequency (Fs)	Fs = N/A	Horton [8]	
Drainage texture (Rt)	T = Dd* Fs	Smith [57]	
Form factor (Rf)	$Rf = A/Lb^2$	Horton [8]	
Elongation ratio (Re)	$Re = 1.128*A^{1/2}/Lb$	Schumm [58]	
Circulatory ratio (Rc)	$Rc = 4\pi A/P^2$	Miller [59]	
Relief aspect			
Relief ratio (Rr)	Rr = H-h/Lb	Schumm [58]	

Channel change analysis

Channel changes were analyzed for the downstream reach in the floodplains of Assam. For assessing channel and planform changes the entire channel length, from the confluence of Mangde and Manas slightly upstream of Mathanguri, up to the confluence point of Manas-Beki with the Brahmaputra river, was divided into reaches, and cross-sections were generated at every 5 km channel length (Figure 2.2). Actual channel paths comprising the river thalweg, left and right banks were extracted for 1990, 2000, 2010, and 2020 from satellite images which were orthorectified images of the post-monsoon period enabling the comparison between different years. The channel reach of 2020 was used to generate the 5 km reaches which were named alphabetically as A to T from upstream to downstream for the Manas main channel and $A^{/}$ to $H^{/}$ for the Beki sub-section which separates after Mathanguri and joins into Manas at the NH crossing downstream.

Errors in river planform analysis using satellite data includes the referencing error and error due to digitization. The error due to georeferencing is minimal as orthorectified images of same spatial resolution were used with high accuracy levels. Uncertainty in manual extraction of streamlines from satellite data was attributed by quantifying the shift between repeat extractions of a 30 km length of the river based on Gurnell [28].

Sinuosity, braiding, channel width, channel migration, erosion, and accretion were the parameters associated with channel and planform changes and were assessed at each equidistant section of the river for every year of analysis.

The sinuosity of a river is measured as the ratio of channel length to valley length. Mathematically, Sinuosity, S= l/ L where, l = actual path length and L = the shortest path length [60]. For braiding analysis, total sinuosity and channel count index were estimated. The total sinuosity is the sum of the mid-channel lengths of all the segments in a channel reach, divided by the length of the main channel [61]. The channel count index is a count of the mean number of channel links per cross-section for a given reach [62].

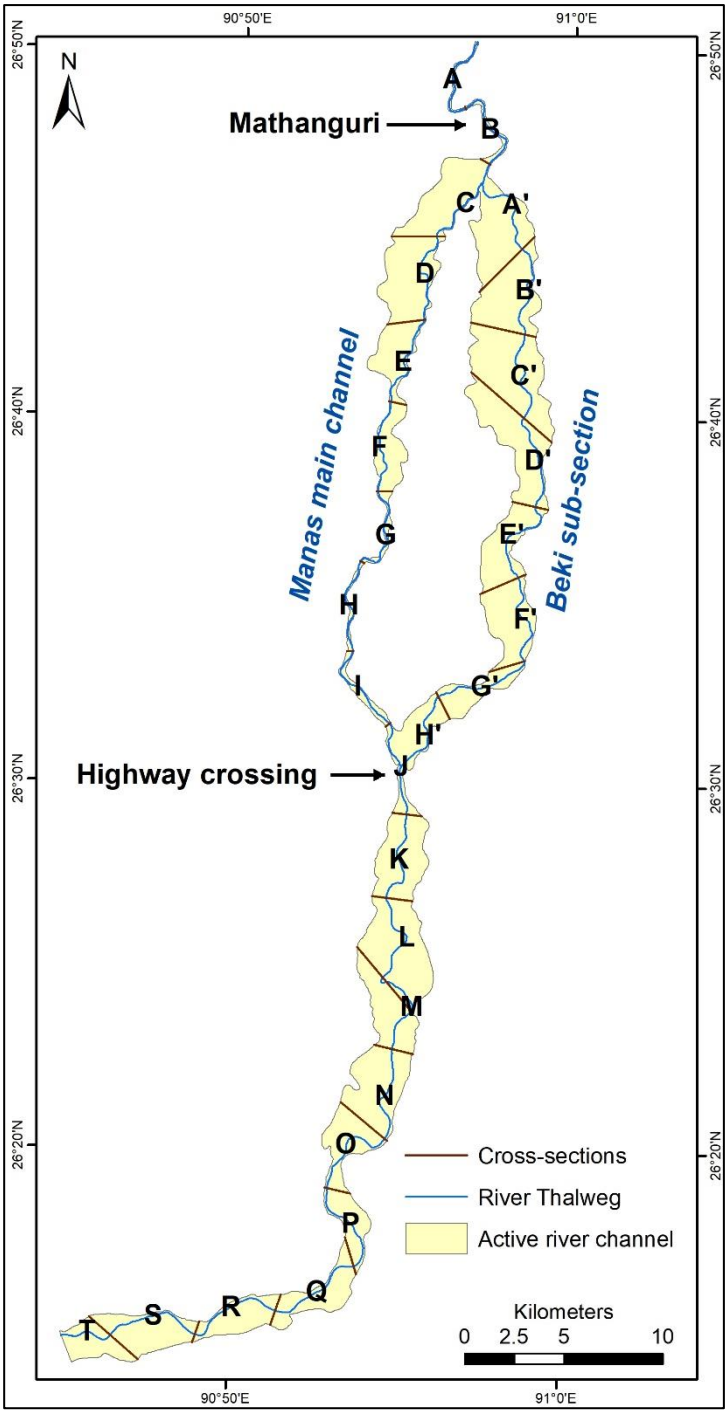

Figure 2.2 Cross-sections and reaches identified for change analysis in Manas-Beki river

Channel width and channel migration were estimated from overlay analysis of the bank lines and river thalweg extracted for four different time periods using geospatial tools. Shift in thalweg, bank lines, and channel width was estimated at each cross-section at the end of every 5 km reach. The areas affected by channel migration resulting in erosion and deposition were estimated for each equidistant 5 km reach by overlaying the bank lines for each year of analysis in GIS software.

2.3 Results

2.3.1 Morphometric analysis

The drainage basin and streams were extracted from SOI toposheets, satellite images, and DEM (Figure 2.3) and basic parameters which are the major inputs for morphometric analysis including area, perimeter, and length of the basin; total number and length of streams; and minimum and maximum basin height were estimated. The hypsometric curve which is a representation of the area within each elevation range of the basin is given in Figure 2.4.

The area of Manas-Beki river basin is estimated to be approximately 32,093 km^2 with a perimeter of 1077 km and a basin length of 301 km. As far as the topographic distribution is concerned, Manas originates in the Tibetan plateau, cuts through the greater Himalayas, and flows through the lesser Himalayas to descend into the Indian plains. The lowest basin height is observed to be around 30 m a.m.s.l in the floodplains and the highest is observed to be 7522 m in the greater Himalayas.

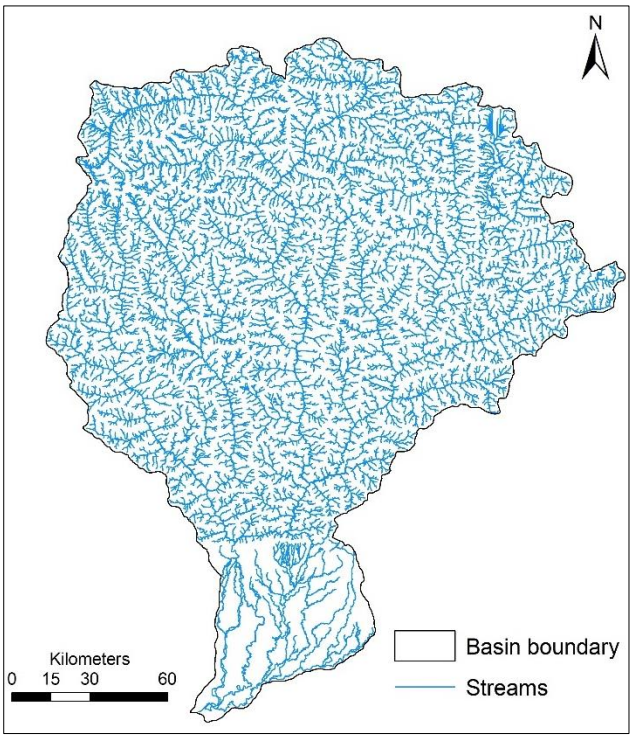

Figure 2.3 Basin boundary and delineated streams of Manas-Beki river basin

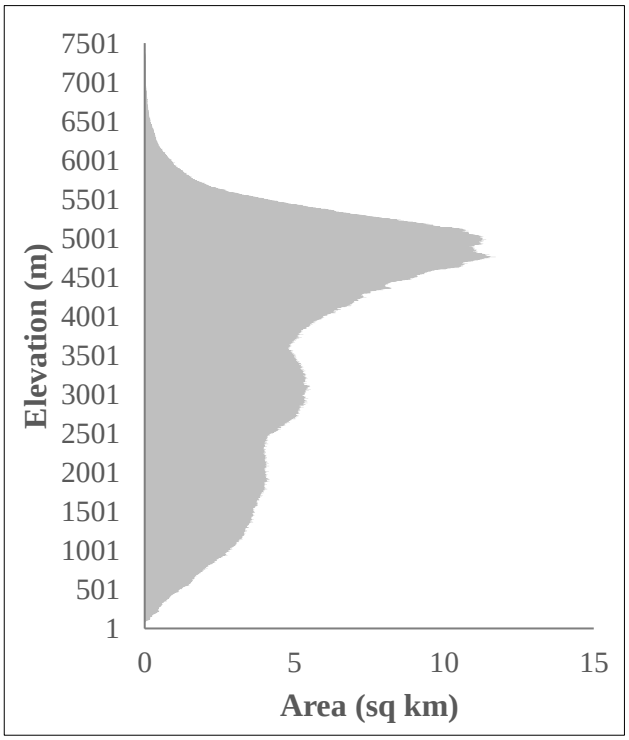

Figure 2.4 Hypsometry of Manas-Beki river system

Linear aspects

Stream order, mean stream length, stream length ratio (Rl), bifurcation ratio (Rb), and Rho co-efficient (ρ) are included in the linear aspects of morphometry. The values derived from morphometric analysis using the established mathematical expressions are presented in Table 2.3.

Table 2.3 Linear aspect of Manas-Beki river basin

Linear parameters	Values estimated
Stream order	10
Mean stream length (Lsm)	0.56 km (±0.0001)*
Stream length ratio (Rl)	1.86
Bifurcation ratio (Rb)	3.97
Rho co-efficient (ρ)	0.47

*Digitization error (quantifies uncertainty in manual extraction)

It is observed that Manas-Beki is a 10^{th} order basin with 213145 streams, out of which 161385 are of the first order which is more than 75% of the total number of streams. The total length of streams is 20747 km and the mean stream length is 0.56 km. Rl is the ratio between the mean lengths of streams in each order to the mean length of streams in the next lower order. Rl between successive stream orders of Manas-Beki is found to have low variations with a mean value of 1.86. Rb is an index of relief and dissections. It is an important parameter that expresses the degree of ramification of the drainage network. Strahler demonstrated that Rb shows only a small variation for different regions in different environments except where powerful geological control dominates [63]. The Rb for Manas-Beki river basin ranges from 1.7 to 4.9 for different order streams with an average of 3.97. This indicates very less to no geological control on the drainage development of the study basins. ρ-co-efficient is influenced by climatic, geologic, biologic, geomorphologic, and anthropogenic factors. The higher value of ρ indicates a greater length of larger stream channels, which may afford increased channel water capacity as compared to a drainage basin with the same drainage density and a lower value of ρ [56]. The ρ value of 0.47 for Manas-Beki indicates a moderate water storage potential.

Areal aspects

Areal aspects include drainage density (Dd), stream frequency (Fs), drainage texture (Rt), form factor (Rf), elongation ratio (Re), and circulatory ratio (Rc). The values of these parameters for the Manas-Beki river basin are presented in Table 2.4.

Dd is a result of interacting factors controlling the surface runoff and is a component influencing the output of water and sediment from the drainage basin [12]. Dd also gives an idea about the physical properties of the underlying rock of a basin. The drainage network of the basin (Figure 2.3) shows that Dd varies significantly within the basin. Dd is much lower in

the foothill and adjoining plains. Changes in slope, dense vegetation cover, and permeability difference play a key role in Dd variation as the upper hill is less permeable than the lower alluvial plains.

Table 2.4 Areal parameters of Manas-Beki river basin

Areal parameters	Values estimated
Drainage density (Dd)	3.71 (±0.0008)*
Stream frequency (Fs)	6.64
Drainage texture (Rt)	24.66 (±0.006)*
Form factor (Rf)	0.35
Elongation ratio (Re)	0.67
Circulatory ratio (Rc)	0.34

*Digitization error (quantifies uncertainty in manual extraction)

Fs is another parameter that is mainly dependent on the lithology of the basin and reflects the texture of the drainage network [64]. Fs is calculated as 6.6 for the Manas-Beki basin which makes the basin moderately sensitive to changes in overland flow. Again, the difference in drainage density between the hilly catchment and plains indicates that though runoff will be quickly transported through the hills, the low stream frequency and low slope in the plains will result in flooding.

Rt is the product of drainage density and stream frequency, and it depends on factors such as climate, rainfall, vegetation, rock, soil type, infiltration capacity, relief, and stage of development of a basin [57]. Rt value of the Manas-Beki river basin estimated to be 24.66 can be categorized as ultra-fine drainage texture. Rt represents the relative spacing between channels and the value is different for the hilly region and the plains which has much bigger spacing suggesting higher overland flow.

Shape factor for a basin is important to understand flood discharge in time and space. It includes Rf, Re, and Rc. Rf value indicates the flow intensity of a basin of a defined area and is defined as the ratio of basin area to the square of basin length [56]. The value for a perfectly round basin is 0.75. The Rf value for Manas-Beki basin is 0.35 indicating a moderately elongated basin with lower peak flows of longer duration than average. Re is another shape parameter that is defined as the ratio between the diameter of the circle of the same area as the drainage basin and the maximum length of the basin [58]. Depending on the Re value, basins are

generally grouped into 3 categories- circular (>0.9), oval (0.9 to 0.8), and less elongated (<0.7). The value of Re for Manas-Beki river basin is 0.67 which indicates the less elongated nature of the basin. Re values in the range of 0.6–0.8 are usually associated with high relief and steep ground slopes [54]. Rc is defined as the ratio of the basin area to the area of a circle having the same circumference as the perimeter of the basin [59]. It is influenced by the length and frequency of streams, geological structures, land use/land cover, climate, relief, and slope of the basin. Low, medium, and high values of Rc indicate the young, mature, and old stages of the life cycle of a watershed [64]. Rc of the Manas-Beki river basin is estimated to be 0.34 indicating a less circular basin and is suggestive of being in the youthful stage of topographical maturity.

Relief aspects

The slope of a basin influences the morphometric as well as hydrogeomorphic characteristics of a basin. It affects the runoff, recharge, and movement of surface water [65] and also determines the drainage pattern of a basin [66, 67]. The slope of the basin has been categorized into 5 classes: level (0^0–10^0), gentle (10^0–20^0), moderate (20^0 – 30^0), steep (30^0 – 45^0), and very steep slope (>45^0). For the Manas-Beki basin, the slope varies from level to gentle in the plains whereas moderate to very steep in the hills (Figure 2.5). Around 60% of the basin has moderate to very steep slopes and 18% of the basin comprises of level slope of less than 10^0.

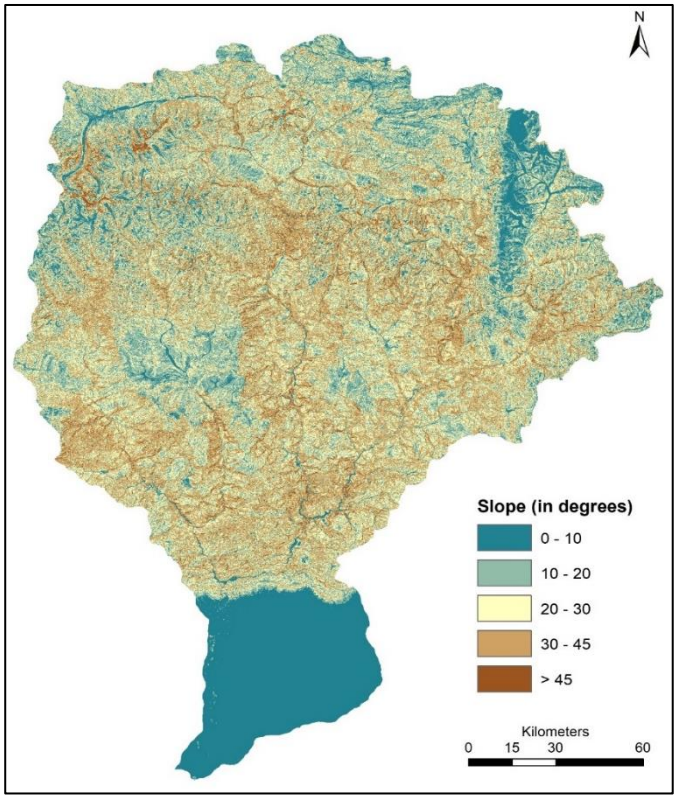

Figure 2.5 Distribution of different slope classes in Manas-Beki river basin

The other factor representing the steepness of terrain is the relief ratio (Rr). It is the dimensionless height-length ratio defined as the ratio of the difference in height between the highest and the lowest points to the basin perimeter [60]. It gives an indication of the intensity of the erosion process operating on the slopes of the basin [64]. Rr of the Manas-Beki basin is 0.02 indicating the basin has a moderate discharge capacity. The plain of the basin generally has a gentle slope. The

low gradient makes the river water spread for a long time over the surface before it gets drained out to the nearest channel causing prolonged flood events. However, in the upper portion, the steep slope favours very high erosion and sediment transport.

2.3.2 Channel and planform changes

The river reach from the Indo-Bhutan border to the confluence with the Brahmaputra can be distinctly identified in two different zones (Figure 2.6): the zone above the National Highway (NH) crossing and the zone below it.

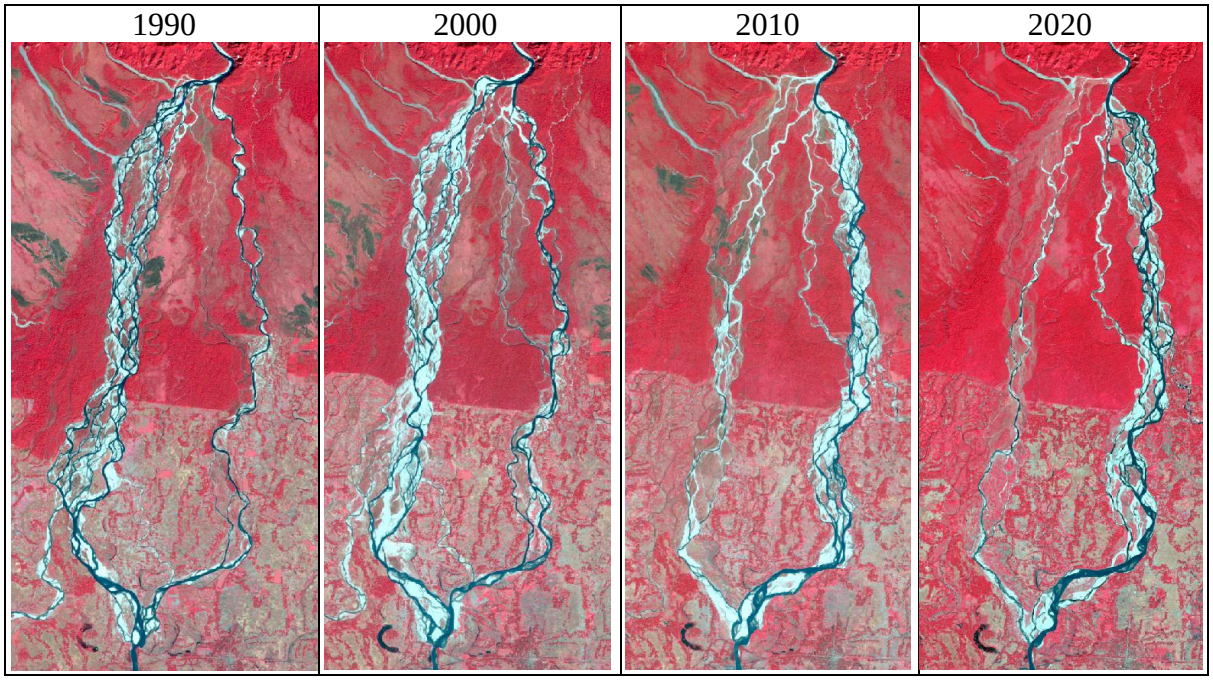

Figure 2.6(a) Landsat satellite images showing the foothills region of the Manas-Beki river

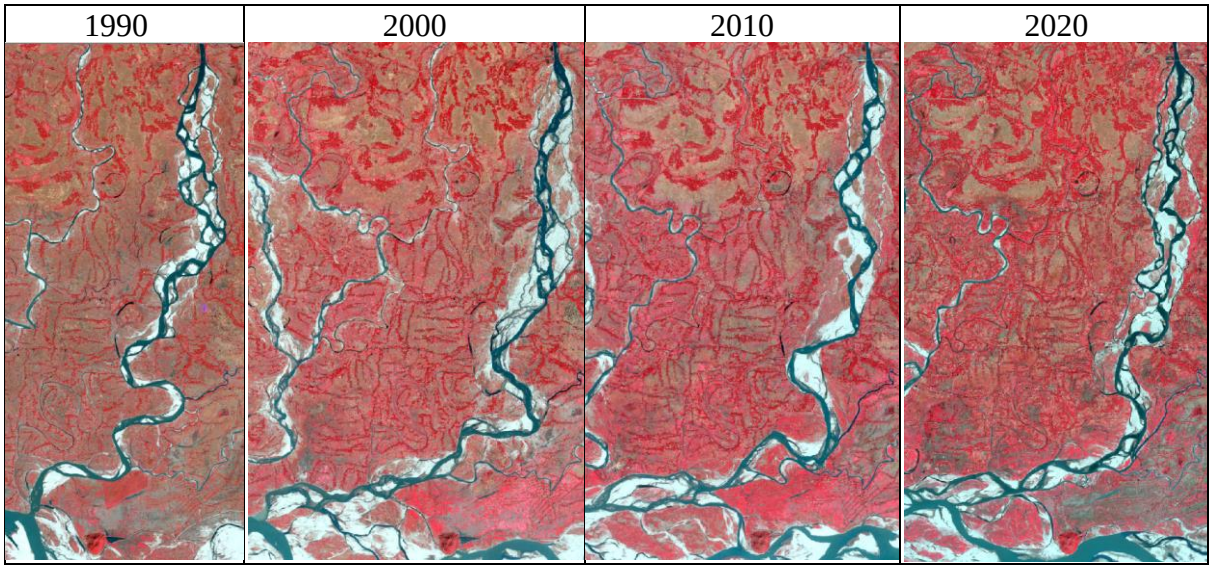

Figure 2.6(b) Landsat satellite images showing the confluence region of the Manas-Beki river

2.3.2.1 Sinuosity and braiding intensity

Sinuosity changes

Channel patterns in plains can be studied through various parameters, and channel sinuosity is one of the measurements of the intensity of channel meanders [60]. Sinuosity was calculated for the divided 5 km reaches of the Manas-Beki river in 1990, 2000, 2010, and 2020. The estimated values for each reach are given in Table 2.5 and the overall changes in sinuosity values for the entire stretch are given in Figure 2.7. Figure 2.8(a) and 2.8(b) show the sinuosity values for each reach in Manas main channel and Beki sub-section respectively.

Table 2.5 Sinuosity values estimated for floodplain reach of Manas-Beki river, 1990-2020

Reach ID	**Sinuosity Index**			
	1990	**2000**	**2010**	**2020**
A	1.49	1.45	1.49	1.47
B	1.73	1.73	1.63	1.64
C	1.18	1.07	1.12	1.11
D	1.09	1.14	1.17	1.18
E	1.14	1.11	1.06	1.12
F	1.12	1.20	1.15	1.10
G	1.16	1.27	1.28	1.38
H	1.21	1.15	1.07	1.10
Reach ID	**Sinuosity Index**			
	1990	**2000**	**2010**	**2020**
I	1.12	1.15	1.20	1.22
J	1.14	1.27	1.14	1.07
K	1.08	1.13	1.14	1.16
L	1.44	1.17	1.20	1.25
M	1.15	1.14	1.30	1.37
N	1.12	1.20	1.11	1.10
O	1.16	1.23	1.16	1.30
P	1.74	1.18	1.10	1.20
Q	2.22	1.13	1.80	1.10
R	1.49	1.13	1.25	1.19
S	1.20	1.20	1.11	1.17
T	1.09	1.12	1.06	1.11
U		1.19	1.03	
A'	1.26	1.18	1.16	1.29
B'	1.24	1.22	1.25	1.16
C'	1.10	1.14	1.20	1.19
D'	1.25	1.14	1.06	1.11
E'	1.18	1.28	1.22	1.36
F'	1.19	1.13	1.11	1.18
G'	1.36	1.31	1.10	1.07
H'	1.15	1.24	1.18	1.13
Overall*	**1.416**	**1.407**	**1.400**	**1.399**
(*Uncertainty = ±0.00033)				

The overall sinuosity of the Manas-Beki river in the floodplain area is decreasing from 1990 to 2020. A slight decrease in the sinuosity indicates a gradual straightening over the years but the values remain less than 1.5. The sinuosity value ranging between 1 to 1.5 indicate an immature river with very high eroding potential and a value greater than 1.5 indicate a mature river with high depositional potential [68]. The sinuosity of Manas–Beki suggests that this system has high erosional potential. On analysis of the values for individual 5 km reaches, it is observed that sinuosity is slightly higher before the river reaches the floodplain region and before the mouth. In other reaches the sinuosity is highly variable but exhibits no noticeable trend and remains mostly between 1.1 and 1.3.

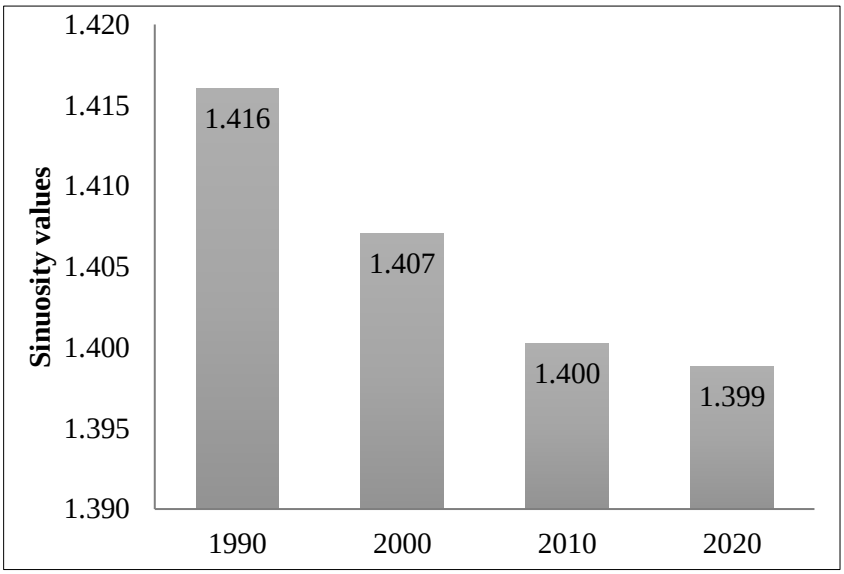

Figure 2.7 Sinuosity values from 1990 to 2020 for the floodplain reach of Manas-Beki river

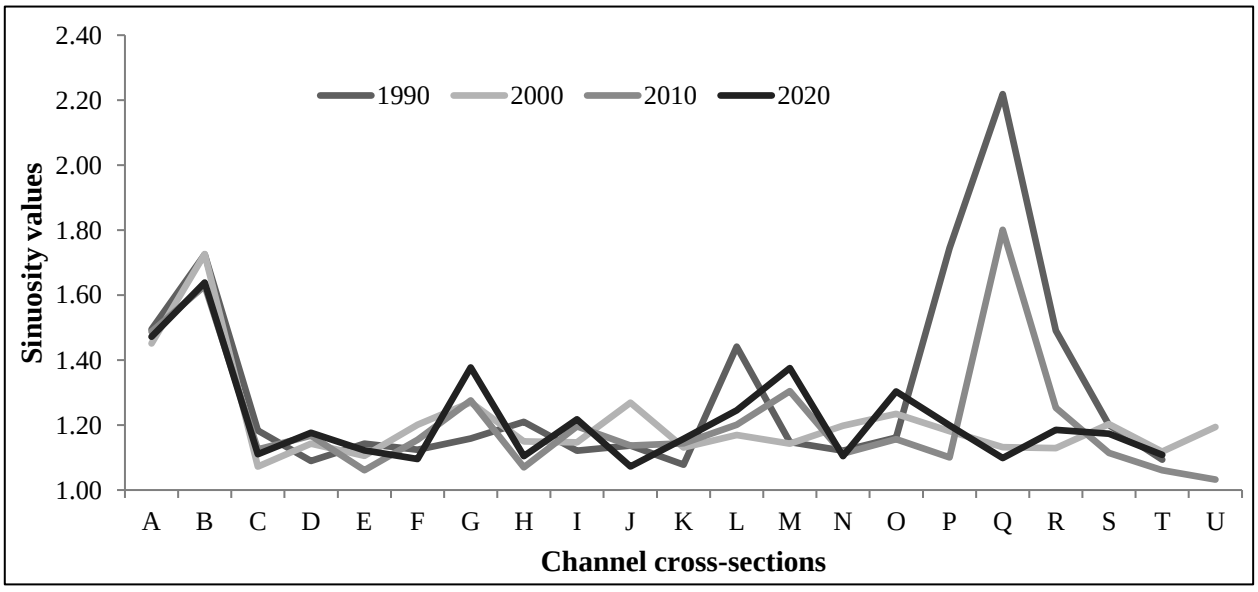

Figure 2.8(a) Sinuosity values from 1990 to 2020 for the Manas main channel

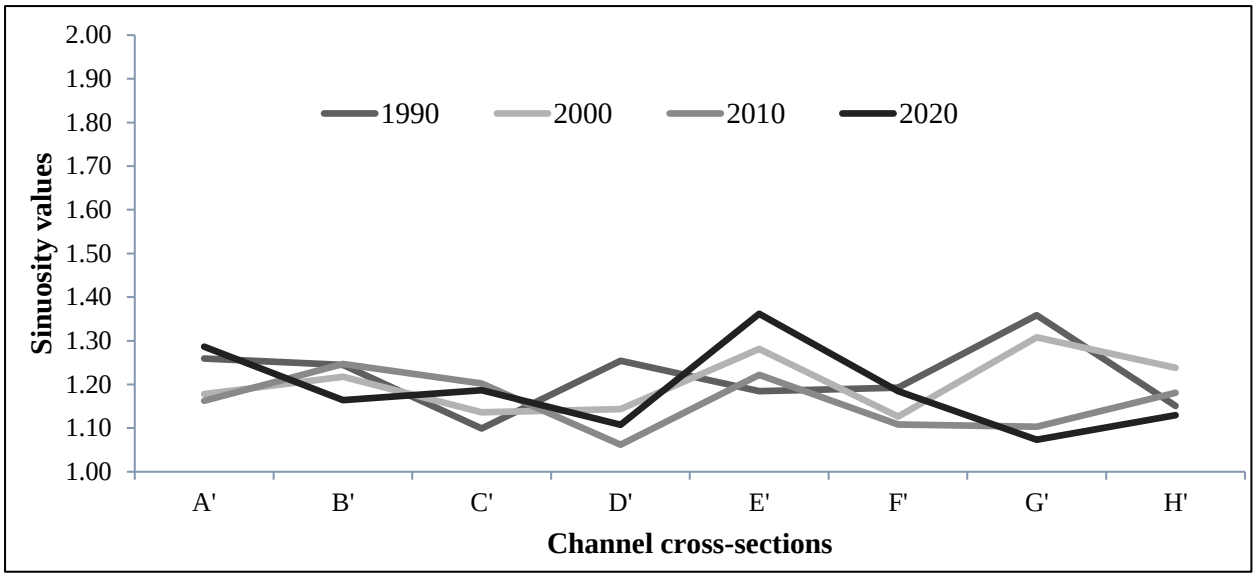

Figure 2.8(b) Sinuosity values from 1990 to 2020 for the Beki sub-section

Changes in braiding intensity

Two commonly applied indices to measure the braiding intensity of a river, total sinuosity and channel count index [68], were also calculated for the selected lower reach of the Manas-Beki river. The total sinuosity is the sum of the mid-channel lengths of all the segments in a channel reach, divided by the length of the main channel [61]. For non-braided rivers, the total sinuosity will be 1 which is the lowest possible value. Higher values denote high braiding intensity. The values of total sinuosity were calculated for 1990, 2000, 2010, and 2020 for every 5 km reach of the floodplain stretch of the Manas-Beki river. The estimated values are presented in Table 2.6 for each reach and Figure 2.9 shows the overall change in total sinuosity values for the entire floodplain stretch as well as Manas main channel and the Beki sub-section. The individual values for each reach of Manas main channel are shown in Figure 2.10(a) and for the Beki subsection in Figure 2.10(b).

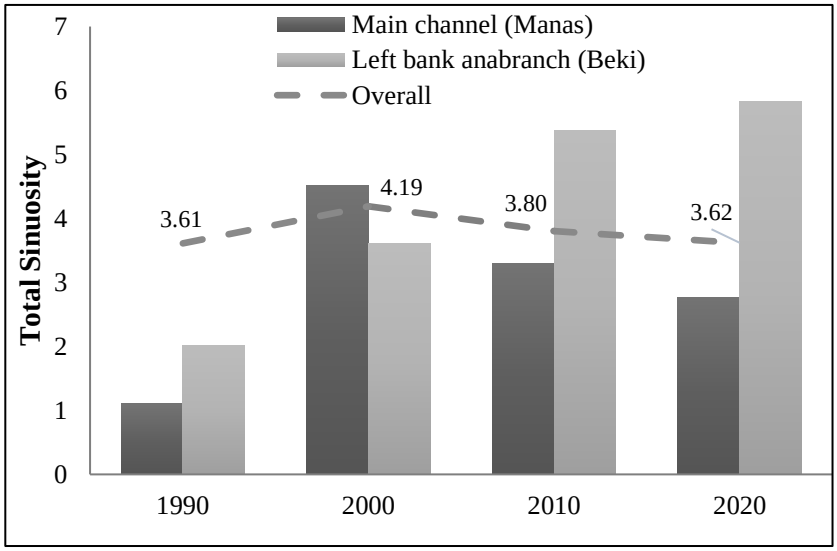

Figure 2.9 Total sinuosity values from 1990 to 2020 for the floodplain reach of Manas-Beki river

Table 2.6 Total sinuosity values estimated for floodplain reach of Manas-Beki river, 1990-2020

Reach ID	Total Sinuosity			
	1990	**2000**	**2010**	**2020**
A	1.00	1.00	1.00	1.00
B	1.00	1.00	1.00	1.00
C	5.73	5.81	3.21	3.83
D	10.32	7.66	6.04	4.46
E	8.13	8.60	3.39	2.39
F	7.62	6.37	4.51	3.85
G	3.80	4.79	4.56	1.80
H	12.05	8.61	3.30	1.40
I	2.82	3.71	1.61	1.14
J	2.30	3.73	1.87	1.58
K	6.01	4.75	5.53	4.66
L	4.01	6.49	3.32	5.17
M	4.20	6.21	3.47	4.39
N	4.17	4.69	3.45	4.24
O	3.02	4.97	2.71	2.67
P	1.59	2.55	2.23	1.81
Q	1.32	1.89	4.43	3.67
R	1.91	3.31	2.37	2.33
S	1.60	2.45	4.20	2.01
T	2.39	2.54	4.78	1.50
U		2.03	1.64	
A'	1.02	3.58	5.95	6.81
B'	1.48	3.85	8.15	6.96
C'	2.63	7.05	4.82	7.90
D'	1.63	3.04	6.52	6.50
E'	2.05	3.09	5.56	5.88
F'	2.48	3.61	6.25	5.84
G'	1.91	2.30	2.48	2.83
H'	2.92	1.85	1.93	3.76
Overall	**3.61**	**4.19**	**3.80**	**3.62**
Manas	1.10	4.51	3.30	2.77
Beki	2.02	3.61	5.38	5.83

The total sinuosity increases from 1990 to 2000 after which it decreases to 2020 for the entire floodplain stretch. The values increase initially between 1990 to 2000 and then decrease from 2000 to 2020 for the Manas main channel but the Beki sub-section shows an increase over the years. On analysis of the individual values for each 5 km reach, it is observed that the total sinuosity decrease for the Manas main channel and increase for the left bank anabranch till the NH crossing, after which no significant trend is observed over the years on the downstream reaches till the Brahmaputra confluence.

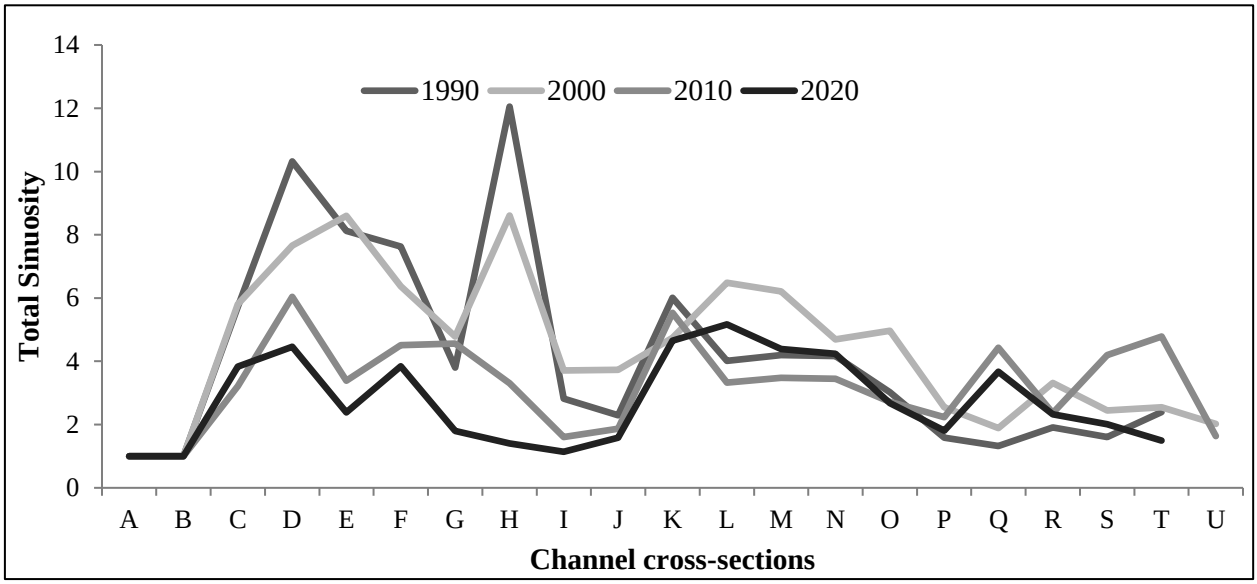

Figure 2.10(a) Total sinuosity values from 1990 to 2020 for the Manas main channel

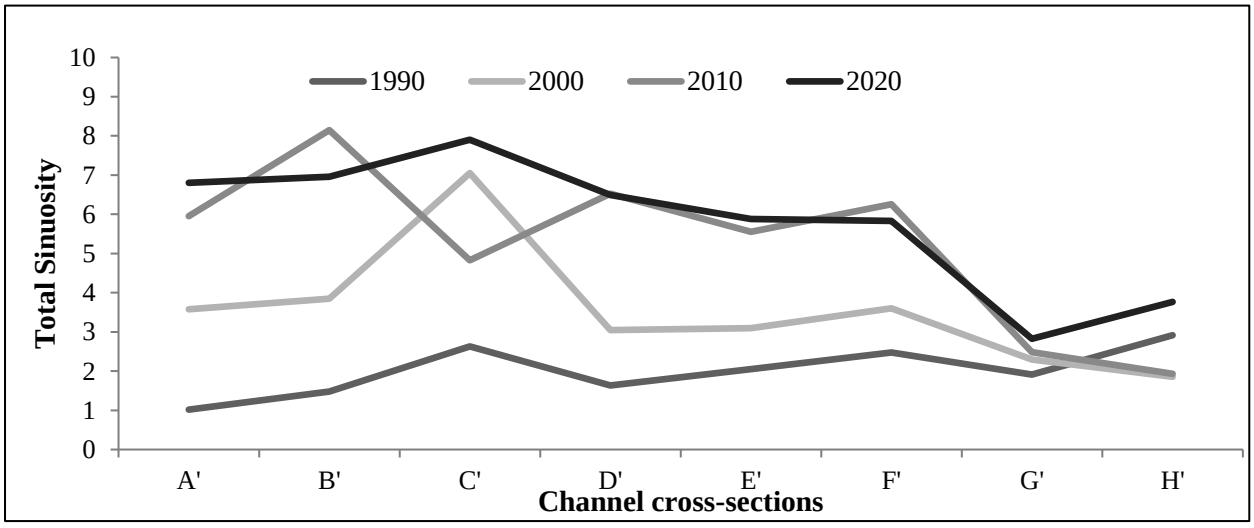

Figure 2.10(b) Total sinuosity values from 1990 to 2020 for the Beki sub-section

The channel count index is a count of the mean number of channel links per cross-section for a given reach and is calculated for each cross-section generated at every 5 km downstream for the floodplain stretch of the Manas-Beki. The cross-sections are named similarly as the reaches were named. High values of channel count index signify higher braiding intensity. The estimated channel count index values are presented in Table 2.7 for each cross-section, and Figure 2.11 shows the overall change in the values for the entire floodplain stretch, Manas main channel and the Beki sub-section. The individual values for each cross-section of Manas main channel are shown in Figure 2.12(a) and for Beki subsection in Figure 2.12(b).

The channel count index increases from 1990 to 2000 after which it decreases to 2020 as also observed for total sinuosity. When the sub-sections are separately analyzed, it is observed that channel count decreases gradually for the main channel while it increases for the Beki sub-section. The change in channel count does not have any specific trend downstream of the road crossing similar to the observations of total sinuosity.

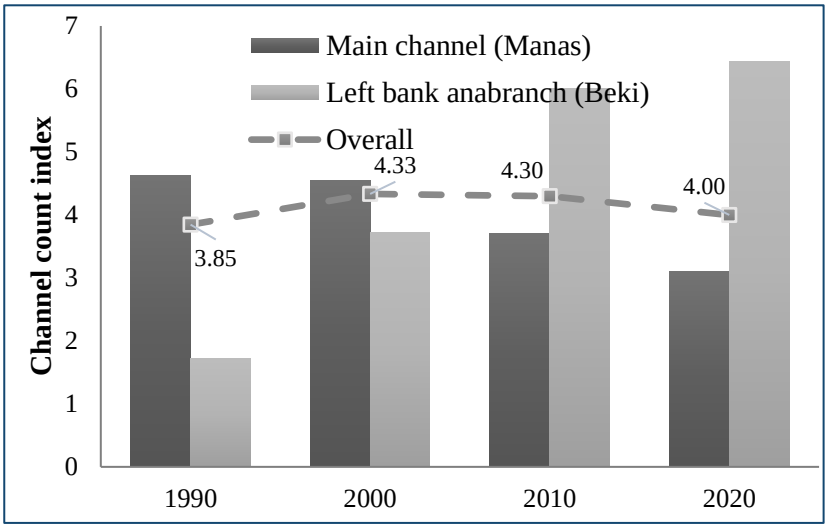

Figure 2.11 Changes in values of channel count index in Manas-Beki basin from 1990 to 2020

Table 2.7 Channel count index for floodplain reach of Manas-Beki river, 1990-2020

XS ID	Channel Count Index			
	1990	2000	2010	2020
A	1	1	1	1
B	3	2	3	3
C	7	10	4	4
D	13	8	5	4
E	9	7	3	2
F	4	4	4	4
G	13	10	6	1
H	3	6	1	2
I	3	3	3	2
J	1	1	7	3

K	5	7	4	5
L	5	7	3	6
M	6	7	4	6
N	4	5	3	3
O	2	3	4	2
P	2	2	2	2
Q	2	1	4	3
R	3	3	4	1
S	2	1	6	5
T		3	3	
A'	1	4	7	10
B'	1	6	8	5
C'	3	4	7	9
D'	1	2	5	5
E'	1	6	9	10
F'	3	2	3	4
G'	2	2	3	2
Overall	**3.85**	**4.33**	**4.30**	**4.00**
Manas	4.63	4.55	3.70	3.11
Beki	1.71	3.71	6.00	6.43

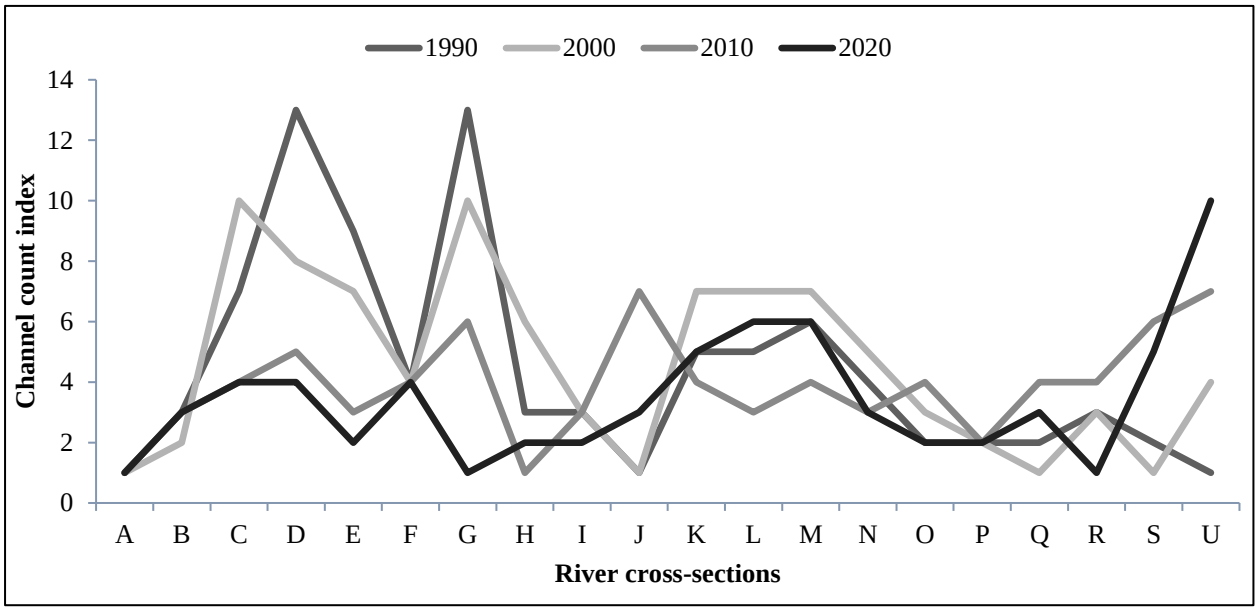

Figure 2.12(a) Channel count index values from 1990 to 2020 for the Manas main channel

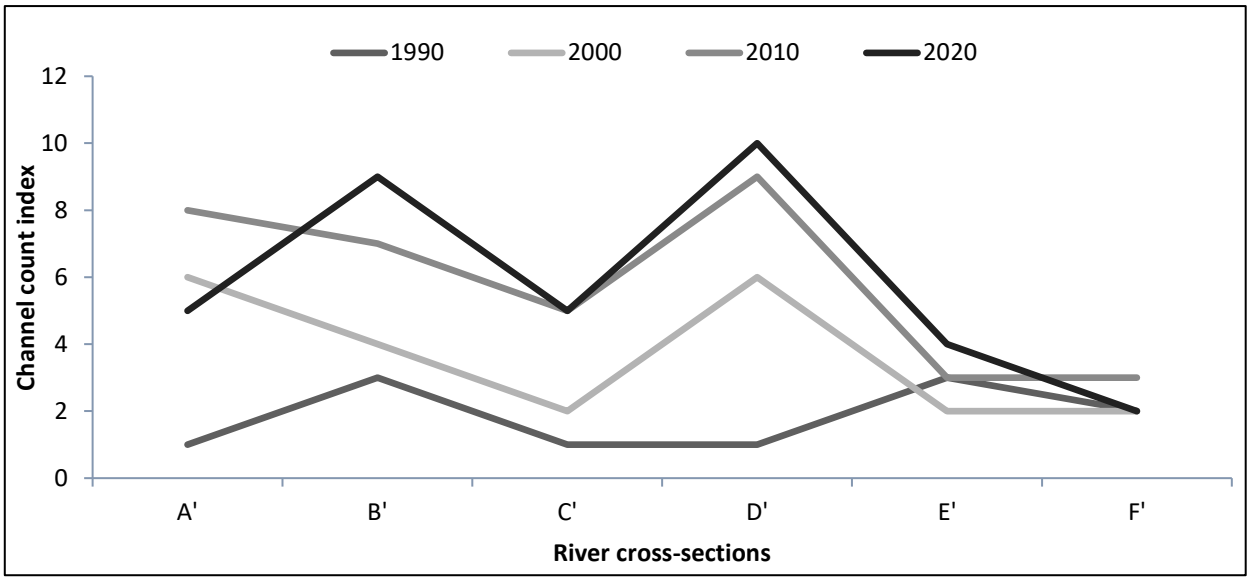

Figure 2.12(b) Channel count index values from 1990 to 2020 for the Beki sub-section

2.3.2.2 Channel change analysis

Thalweg shift

The river thalweg is the continuous line depicting the deepest course of a river. The river thalwegs were identified from the satellite images of 1990, 2000, 2010, and 2020. The shift during each time period was estimated at each of the identified 24 cross-sections in the floodplain stretch of the Manas-Beki river. Figure 2.13(a) shows the map of thalwegs of the Manas-Beki river for the reach from Mathanguri to NH crossing and Figure 2.13(b) shows the thalwegs from NH crossing to the Brahmaputra confluence for the different time periods of analysis.

The most significant change in river thalweg is the shift between 2000 and 2010 from the right bank (Manas) anabranch to the left bank (Beki) anabranch before meeting at the NH crossing downstream. Since the deepest course of the river shifted from the right bank anabranch to the left bank anabranch between 2000 and 2010, the thalweg was not extracted for the years 2010 and 2020 for the right bank anabranch. The magnitude of maximum shift at each cross-section, along with the direction of change for the periods 1990-2000, 2000-2010, and 2010-2020, has been estimated (Table 2.8). The nature of changes and the spatial pattern are depicted in Figure 2.14(a) and 2.14(b) for Manas main channel and Beki sub-section respectively. Eastward shift towards the left bank is indicated in positive and westward shift towards the right bank in negative values.

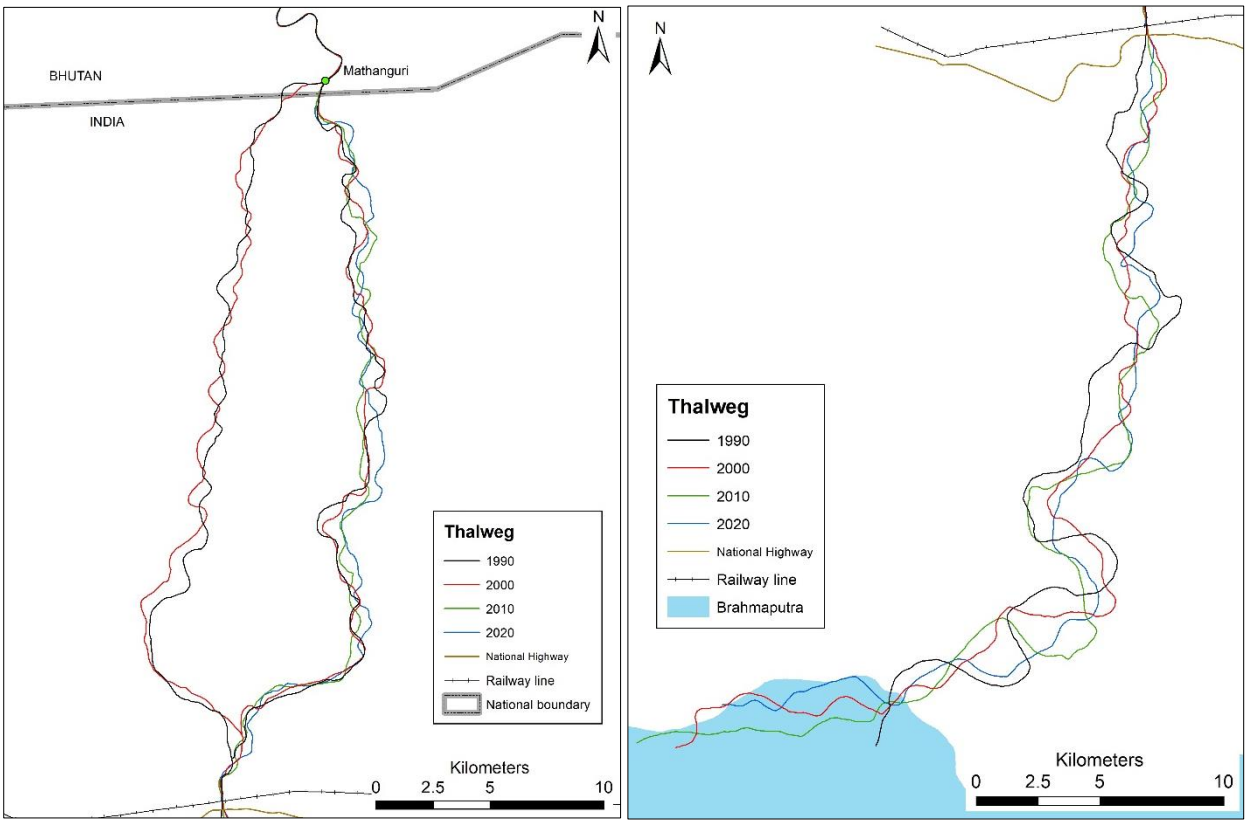

Figure 2.13 River thalwegs from 1990 to 2020 for the (a) upstream reach of NH crossing, and (b) downstream of NH crossing

The values of thalweg shift are not available for cross-sections B to I for 2000-2010 and 2010-2020 as these cross-sections represent the Manas main channel anabranch in the right bank. The values are mostly negative for the cross-sections in the right bank anabranch (Manas) and positive for the left bank anabranch (Beki) indicating a shift of the thalweg towards the left over the years for the reaches upstream of the NH crossing. In the downstream region, the shift is highly erratic with the thalweg shifting erratically between left and right. The maximum overall shift between 1990 and 2020 is more than 2 km in the downstream reach.

Table 2.8 Thalweg shift between 1990 to 2020 for the Manas-Beki river

XS ID	Thalweg shift (m)			
	1990-2000	2000-2010	2010-2020	Overall (1990-2020)
A	-7.21	14.30	-2.99	4.10
B	15.08			15.08
C	-582.57			-582.57
D	245.37			245.37
E	18.05			18.05
F	-298.53			-298.53

G	-532.28			-532.28
H	-258.77			-258.77
I	8.60			8.60
J	597.79	-257.36	79.10	419.52
K	299.36	696.15	-555.26	440.24
L	-800.86	-812.97	1031.13	-582.70
M	535.99	362.33	-464.14	434.17
N	891.66	1286.25	14.43	2192.34
O	1814.17	-1913.78	1057.68	958.07
P	1077.00	-985.68	778.38	869.70
Q	-1468.54	-793.83	1827.81	-434.56
R	304.90	-108.97	134.14	330.08
S		1650.18	-1442.16	208.02
A'	-29.76	-91.21	932.00	811.04
B'	-164.84	433.69	277.22	546.07
C'	294.02	-997.67	89.21	-614.44
D'	-109.26	-309.45	687.10	268.38
E'	-16.17	210.61	664.43	858.87
F'	-12.87	-626.15	611.30	-27.71
G'	-117.80	-260.02	11.51	-366.31

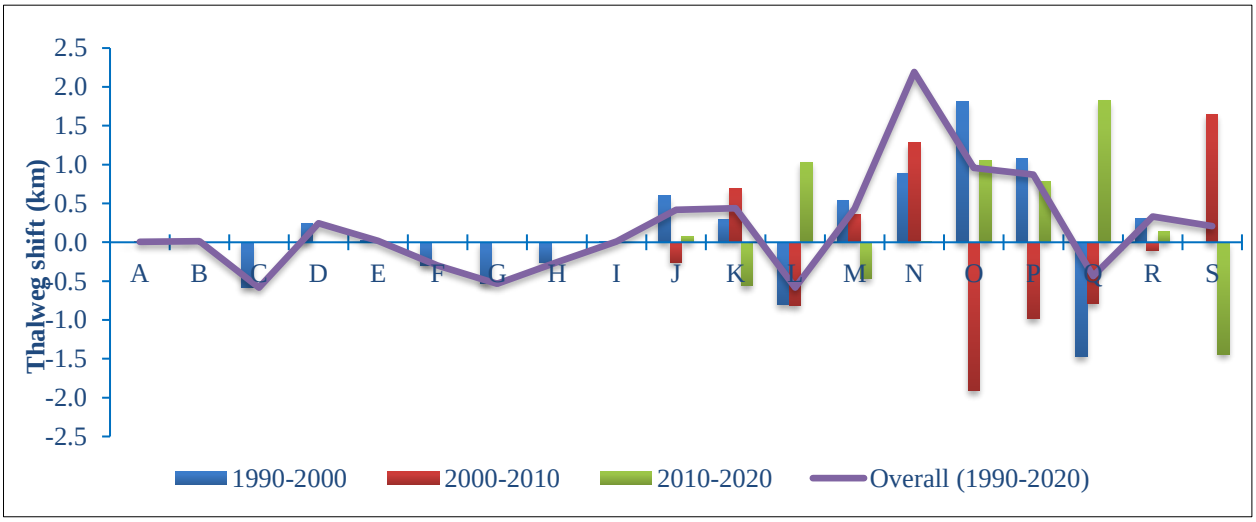

Figure 2.14(a) Thalweg shifts at each cross-section of main channel Manas *(Eastward shift towards the left bank is indicated in positive and westward shift towards the right bank in negative values)*

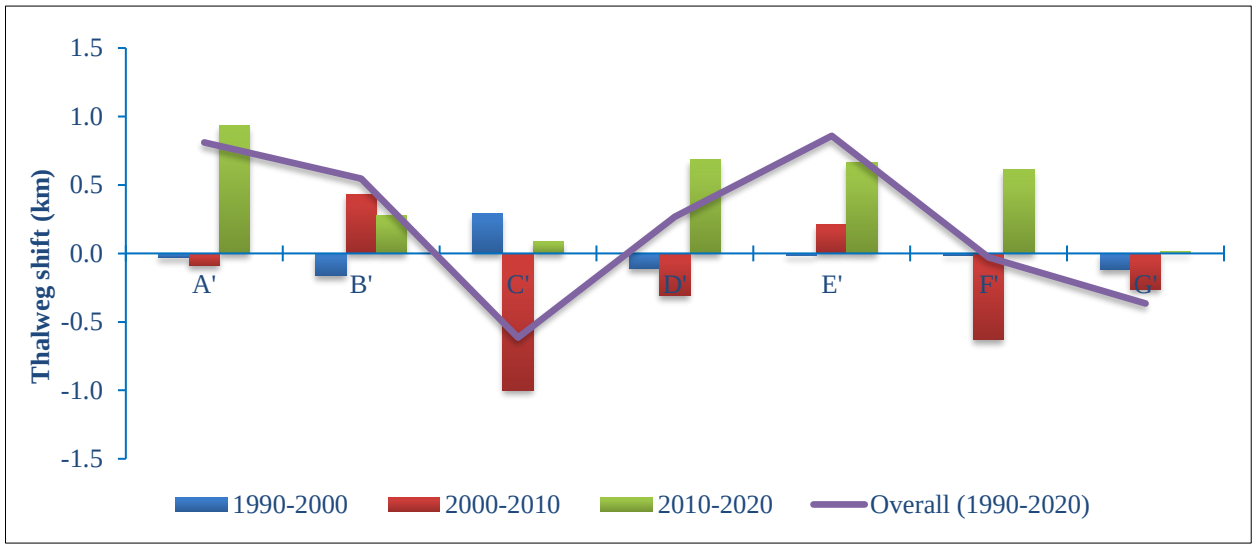

Figure 2.14(b) Thalweg shifts at each cross-section of the Beki sub-section *(Eastward shift towards the left bank is indicated in positive and westward shift towards the right bank in negative values)*

Bank line shift

The river bank lines for the left and right banks were identified from the satellite images of 1990, 2000, 2010 and 2020. Figure 2.15(a) shows the map of identified bank lines of the Manas-Beki river for the reach from Mathanguri to NH crossing and Figure 2.15(b) shows the bank lines from NH crossing to Brahmaputra confluence for the different time periods of analysis. The shift in the left bank and right bank during each time period (1990-2020) was estimated at each of the identified 24 cross-sections in the floodplain stretch of the Manas-Beki river. The magnitude of maximum shift at each cross-section, for the periods 1990-2000, 2000-2010, 2010-2020, and overall change from 1990-2020 has been estimated, and the values of the shift are presented in Table 2.9. The values are taken as positive for an outward shift of bank lines, i.e., right bank shift towards the west and the left bank shift towards the east, whereas the values are taken as negative for an inward shift of bank lines, i.e., when the right bank shift towards the east and left bank towards the west. This is done as an attempt to portray the narrowing or widening of rivers taking place at different times and places. The changes in the left bank of the Manas-Beki river are depicted in Figures 2.16(a) and 2.16(b) for Manas main channel and Beki sub-section respectively. It is observed that between 1990 and 2020, the largest shift in the left bank has been in the downstream region in the order of more than 2 km outwards. In the Beki anabranch sections, the shift is mostly outwards ranging from 130 m to about 1.25 km. For the Manas anabranch reach, the shift is inwards near the point where the anabranches join above the NH crossing.

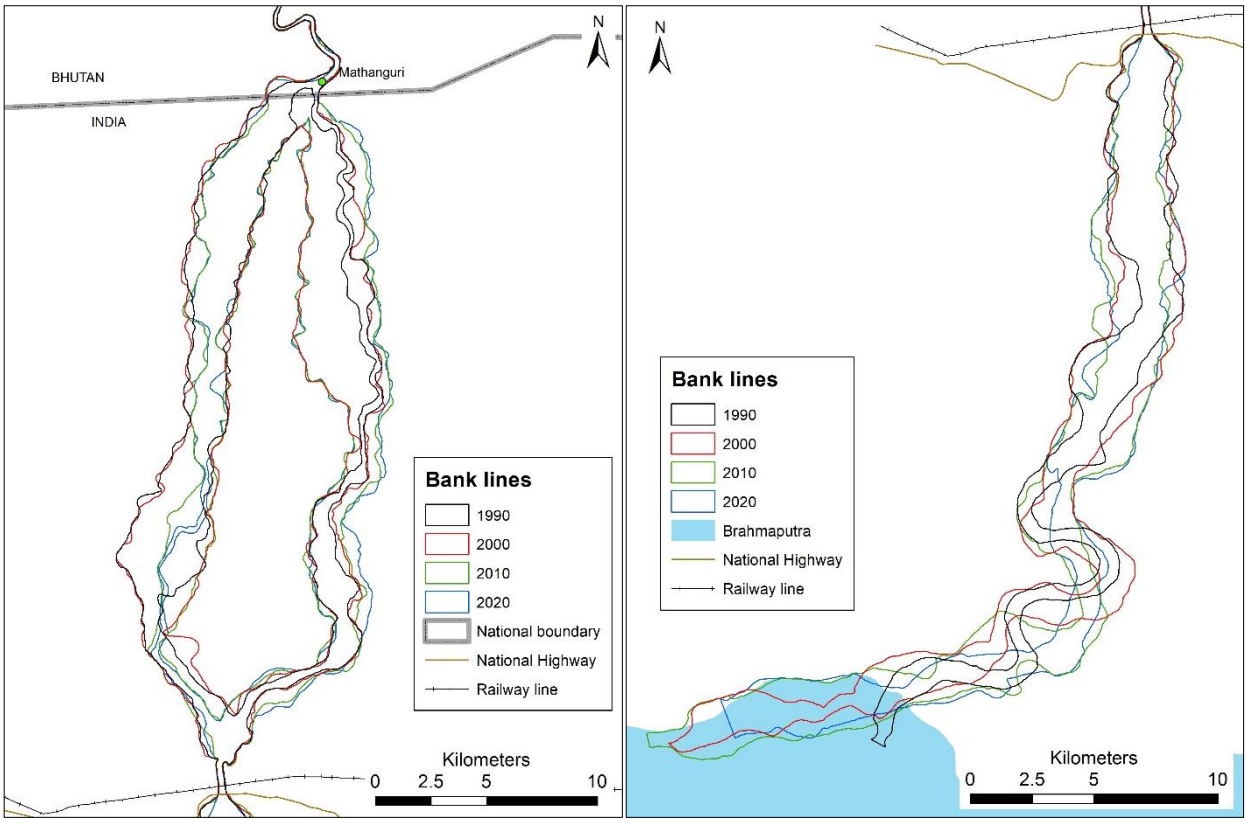

Figure 2.15 River bank lines from 1990 to 2020 for the (a) upstream reach of NH crossing, and (b) downstream of NH crossing

Changes downstream of NH crossing are observed between 1990 and 2000 whereas changes in the Beki anabranch (upstream of NH crossing) are mostly between 2000-2010 and 2010-2020 showing recent changes. Changes in the Manas anabranch reach are comparatively much less mostly in the order of a few meters and confined to the left bank. The changes in the right bank of the Manas-Beki river are depicted in Figures 2.17(a) and 2.17(b) for Manas main channel and Beki sub-section respectively. For the right bank, between 1990 and 2020, the maximum shift is around 1.8 km inwards for the Manas anabranch reach. The shift in right bank for the Beki anabranch region is a maximum of 3.5 km outwards. After the NH crossing, the shift is erratic with a maximum outward shift of ~1.2 km and an inward shift of ~1.3 km. Over the years, the maximum right bank shift is inwards for the Manas anabranch section between 2000 and 2010 and outwards for the Beki anabranch section from 1990 to 2000. The maximum right bank shift downstream of the NH crossing is observed between 2010 to 2020 and the shift is negative indicating an inwards shift.

Table 2.9 Values of bank line shift between 1990 to 2020 for left and right bank of Manas-Beki river

XS ID	1990-2000		2000-2010		2010-2020		Overall (1990-2020)	
	Left bank	Right bank	Left bank	Right bank	Left bank	Right bank	Left bank	Right bank
A	-12.99	-1.08	-0.67	22.86	21.45	-3.17	7.79	18.61
B	-23.41	37.61	-10.16	15.93	12.35	-116.92	-21.22	-63.38
C	-0.64	372.33	66.85	-383.56	1.40	31.92	67.61	20.70
D	39.13	114.28	95.99	-1060.46	27.68	-11.23	162.80	-957.42
E	-14.98	80.39	73.56	-618.51	-29.35	-150.60	29.22	-688.73
F	149.34	-71.44	-12.92	-891.34	-7.40	-6.99	129.02	-969.78
G	565.88	85.06	-81.33	-1633.10	-1353.60	-261.26	-869.04	-1809.30
H	138.50	19.02	306.39	-553.89	-166.17	-209.92	278.73	-744.80
I	84.64	90.81	-882.35	-78.21	36.55	-374.87	-761.16	-362.27
J	232.71	-1.81	120.19	18.15	-387.56	-520.07	-34.67	-503.73
K	-46.84	361.25	-154.73	-372.93	-151.67	153.98	-353.25	142.30
L	-437.21	435.43	-583.13	345.08	717.78	426.27	-302.57	1206.78
M	613.86	145.91	14.02	-303.63	-169.48	-293.13	458.40	-450.86
N	275.39	557.16	1166.82	24.50	63.41	-8.21	1505.62	573.44
O	2404.68	-345.38	-521.06	373.96	134.82	-1393.99	2018.44	-1365.41
P	1105.69	-449.70	220.95	453.14	-399.89	11.59	926.75	15.03
Q	-737.67	1191.80	751.54	541.84	410.21	-1058.14	424.08	675.50
R	-205.67	1083.26	239.59	-209.92	-122.20	-772.18	-88.28	101.16
S			766.58	379.26	0.00	332.64	766.58	711.90
A'	29.04	1721.87	759.08	68.14	139.22	50.48	927.33	1840.49
B'	-234.35	2,152.74	438.36	20.27	-65.07	-20.17	138.94	2152.83
C'	117.48	4021.18	653.58	-444.20	42.35	1.11	813.41	3578.09
D'	52.14	551.27	599.71	18.05	217.25	-9.52	869.10	559.80
E'	424.80	53.08	133.49	343.65	690.82	-51.71	1249.10	345.02
F'	-15.51	38.30	46.43	411.44	-59.78	-153.20	-28.85	296.53
G'	18.54	4.29	663.98	198.79	163.81	146.03	846.33	349.11

Overall, the bank line and thalweg shifts indicate the river had significant changes from 1990 to 2020 and relatively stable sections are rarely observed during the years indicating a highly active fluvial landscape.

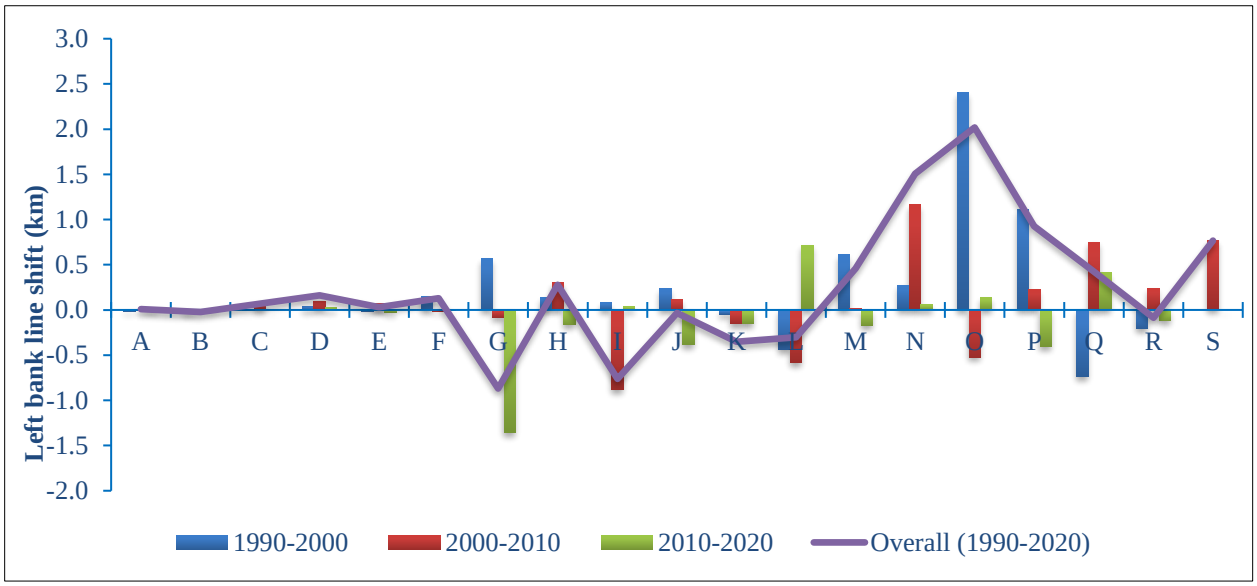

Figure 2.16(a) Bank line shifts in the left bank at each cross-section of main channel Manas *(positive values indicate an outward shift of bank lines, i.e., left bank shift towards the east, and negative values indicate an inward shift of bank lines, i.e., left bank towards the west)*

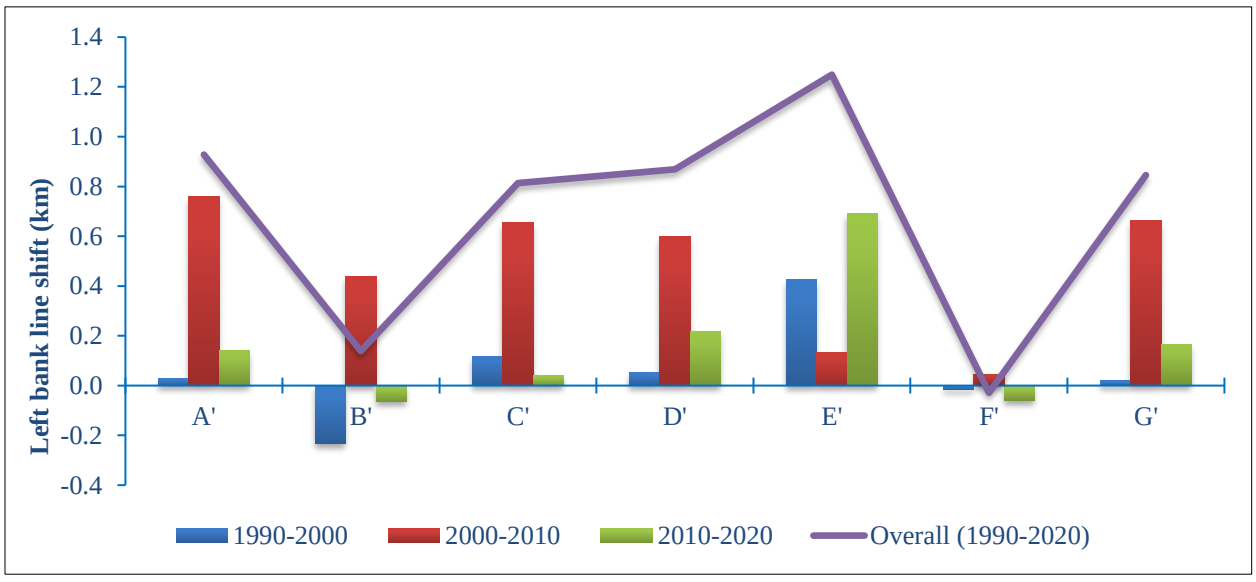

Figure 2.16(b) Bank line shifts in the left bank at each cross-section of Beki sub-section *(positive values indicate an outward shift of bank lines, i.e., left bank shift towards the east, and negative values indicate an inward shift of bank lines, i.e., left bank towards the west)*

Changes in channel width

The changes in channel width have also been analyzed for the different time periods, 1990-2000, 2000-2010, 2010-2020, and overall between 1990-2020 using the bank lines. The values for channel width were measured at each cross-section and are presented in Table 2.10. The change in channel width for each cross-section is shown in Figures 2.18(a) and 2.18(b) for Manas main channel and Beki anabranch section respectively.

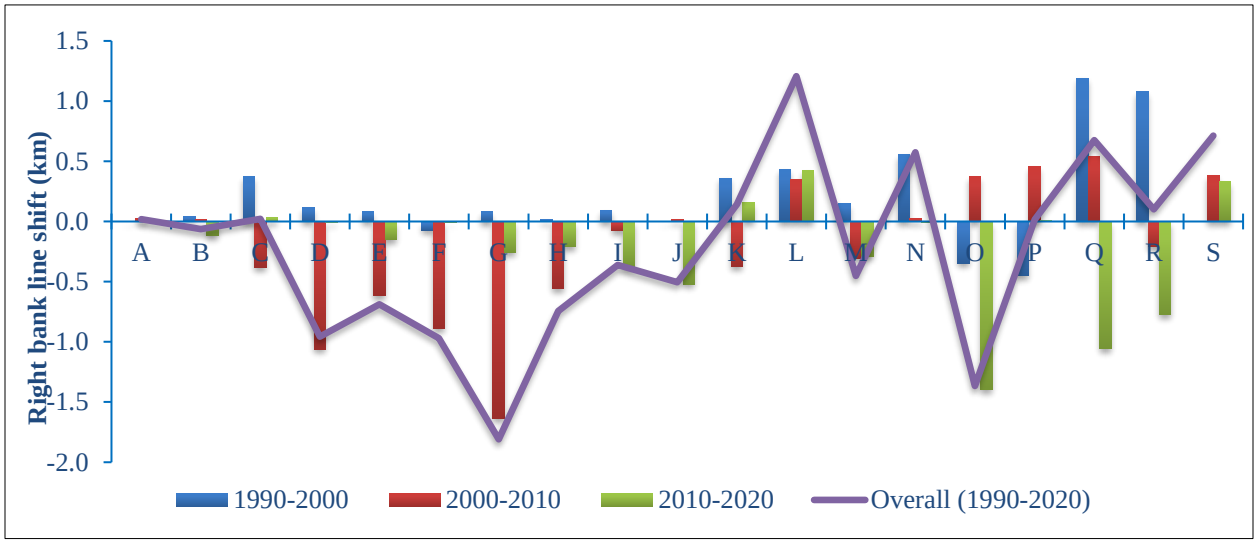

Figure 2.17(a) Bank line shifts in the right bank at each cross-section of main channel Manas *(positive values indicate an outward shift of bank lines, i.e., right bank shift towards the west, and negative values indicate an inward shift of bank lines, i.e., right bank towards the east)*

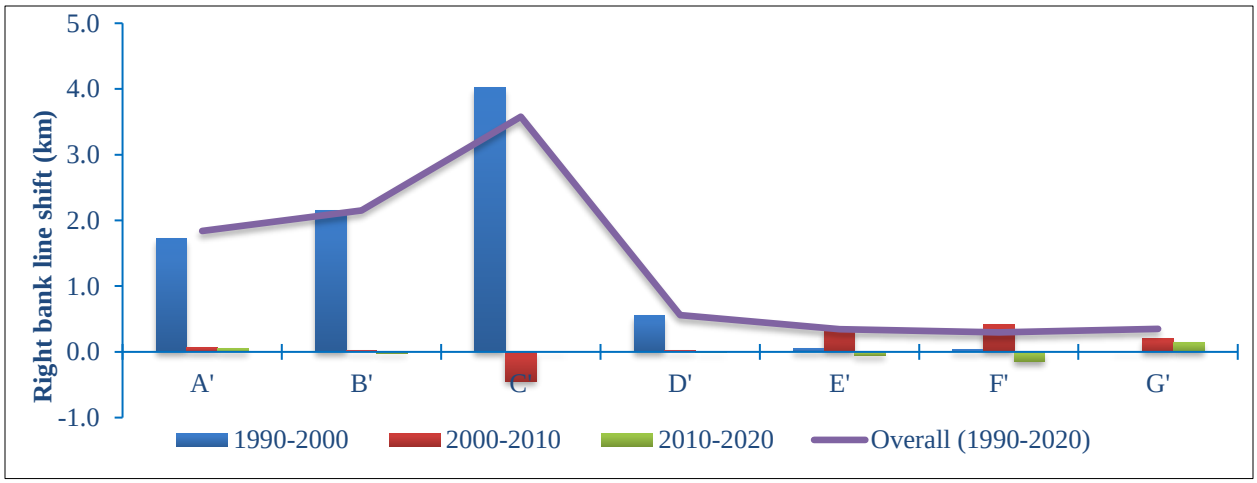

Figure 2.17(b) Bank line shifts in the right bank at each cross-section of Beki sub-section *(positive values indicate an outward shift of bank lines, i.e., right bank shift towards the west, and negative values indicate an inward shift of bank lines, i.e., right bank towards the east)*

Table 2.10 Values of channel width at each cross-section from 1990 to 2020 for Manas-Beki river

XS ID	Change in channel width (m)			
	1990-2000	**2000-2010**	**2010-2020**	**Overall (1990-2020)**
A	-14.08	22.20	18.27	26.40
B	14.20	5.77	-104.58	-84.61
C	371.69	-316.71	33.33	88.31
D	153.41	-964.47	16.45	-794.61
E	65.40	-544.96	-179.96	-659.51
F	77.90	-904.26	-14.39	-840.76
G	650.94	-1714.43	-1614.86	-2678.34
H	157.52	-247.50	-376.09	-466.07
I	175.45	-960.56	-338.31	-1123.42
J	230.90	138.34	-907.63	-538.40
K	314.41	-527.67	2.31	-210.95
L	-1.78	-238.05	1144.04	904.22
M	759.77	-289.61	-462.61	7.55
N	832.55	1191.32	55.20	2079.07
O	2059.31	-147.10	-1259.18	653.04
P	655.99	674.09	-388.31	941.78
Q	454.13	1293.38	-647.94	1099.57
R	877.59	29.67	-894.38	12.88
S	0.00	1145.84	332.64	1478.48
A'	1750.91	827.22	189.69	2767.82
B'	1918.39	458.63	-85.24	2291.77
C'	4138.66	209.37	43.46	4391.49
D'	603.41	617.77	207.72	1428.90
E'	477.88	477.14	639.11	1594.12
F'	22.79	457.87	-212.98	267.68
G'	22.83	862.77	309.84	1195.44

Channel width is observed to be decreasing for the Manas anabranch section and increasing for the Beki anabranch section from 1990 to 2020. The maximum change observed for these sections is a decrease of approximately 2.6 km for the Manas anabranch section and an increase of approximately 4.4 km for the Beki anabranch section from 1990 to 2020. For the section south of the NH crossing, the change is mostly increasing with a maximum increase of around 2 km between 1990 and 2020. The changes are mostly during 2000-2010 and 2010-2020 for the Manas anabranch and during 1990-2000 for the Beki anabranch. South of the NH crossing, the increase

in channel width is observed mostly during 1990-2000 followed by 2000-2010. During 2010-2020 a decrease in channel width is observed in the downstream reaches.

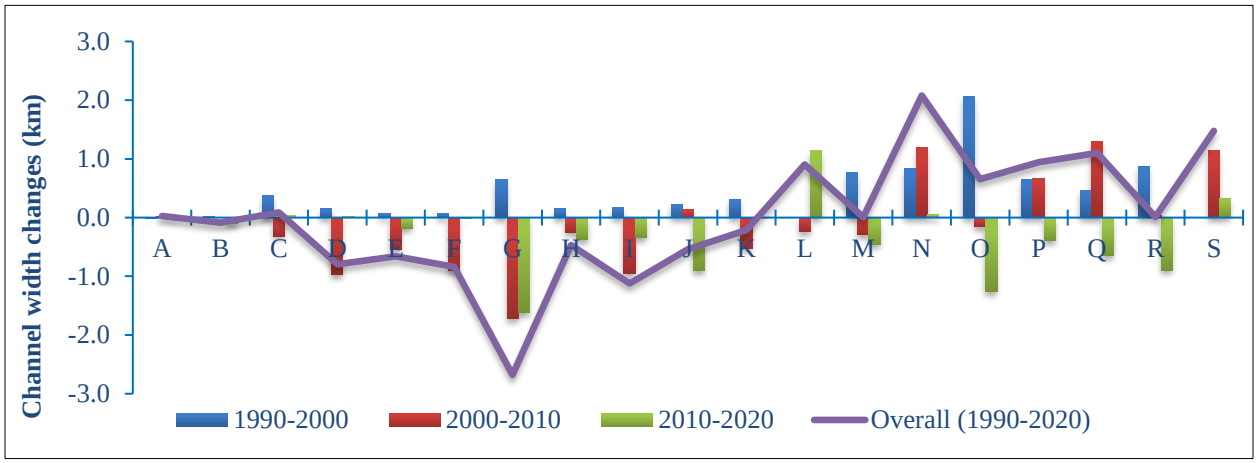

Figure 2.18(a) Changes in channel width at each cross-section of main channel Manas *(positive and negative values indicate channel width increase and decrease respectively)*

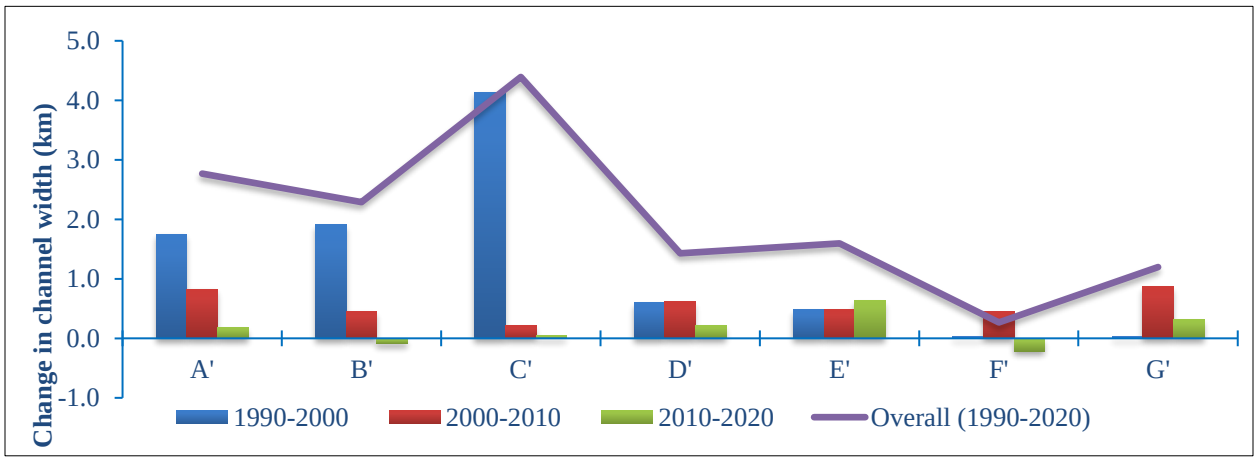

Figure 2.18(b) Changes in channel width at each cross-section of Beki sub-section *(positive and negative values indicate channel width increase and decrease respectively)*

2.3.2.3 Erosion and deposition trends

The differential rates of erosion and deposition due to changes in the river course have been analyzed along the identified 5 km segments for the periods 1990-2000, 2000-2010, and 2010-2020 respectively shown in Figures 2.19(a), 2.19(b) and 2.19(c). The results for each reach for the entire studied stretch of the river during 1990-2000, 2000-2010, 2010-2020, and overall change from 1990-2020 are presented in Table 2.11. The values of erosion are considered as negative as these areas are lost due to channel shift and the values for deposition are considered as positive as

these areas are accretion areas where fluvial deposits are accumulated. The net change in area is also calculated for each period of study. A positive value indicates deposition areas exceed eroded areas and vice versa. The total areas of erosion and deposition for the entire Manas-Beki river for the different time periods of analysis are shown in Figure 2.20. The erosion and deposition areas for each reach are shown in Figure 2.21(a) for the Manas main channel and in 2.21(b) for the Beki anabranch section. The net change in erosion/deposition is also shown graphically to understand the overall dominance of either of the processes in each reach (Figures 2.22(a) and 2.22(b)).

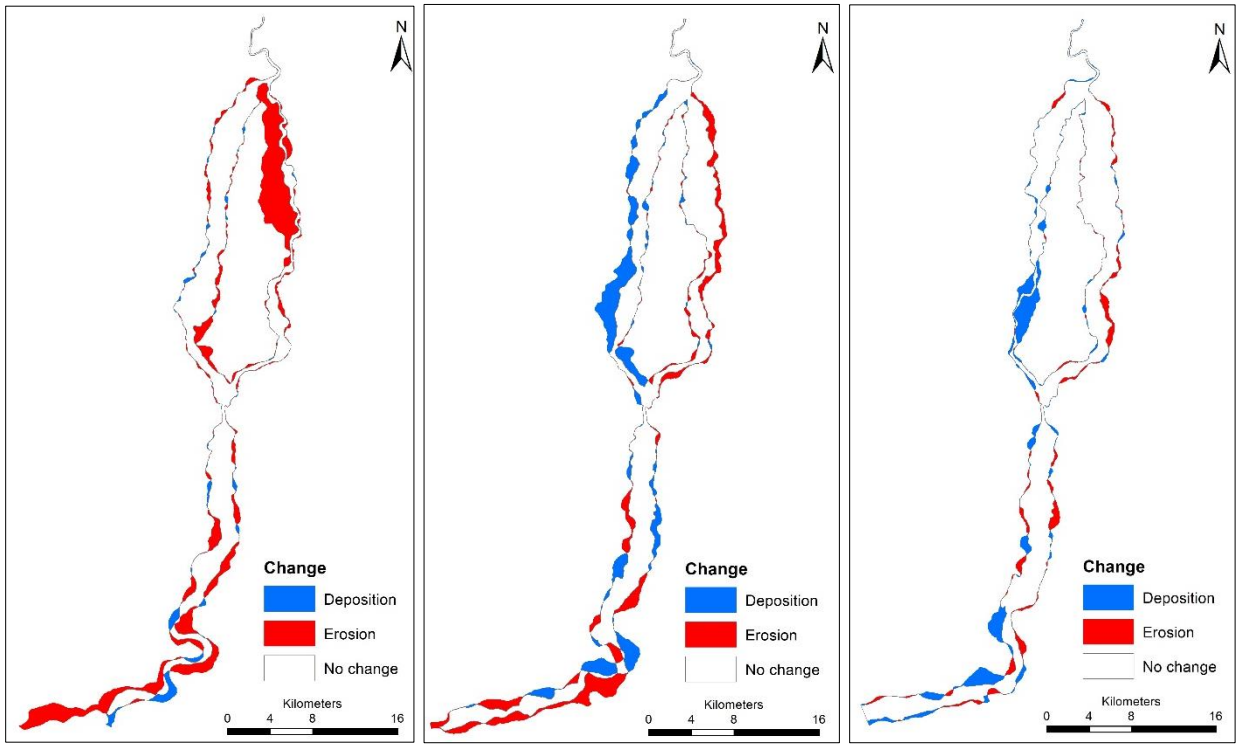

Figure 2.19 Erosion and deposition areas due to changes in river channel course in Manas-Beki river during (a) 1990-2000 (b) 2000-2010, and (c) 2010-2020

During 1990-2020, erosion was high in the Manas-Beki river basin but it shows a decreasing trend over the decades. Deposition was low during 1990-2000 but shows a sharp increase between 2000-2010 and a slight decrease after that. Most of the reaches show high erosion areas in 1990 and high deposition in the other two decades. Erosion is high especially in the lower reach due to avulsion. The lower part of the Manas river is alluvial in nature which easily gets eroded and reshaped by flow making the portion highly prone to erosion. Very high erosion in the Beki anabranch of the

river during 1990-2000 is due to the change in the thalweg line from the right stream to the left resulting in drying of the right stream.

Deposition areas exceed erosion areas during 2000-2010 and 2010-2020 suggesting that deposition is the dominant action of the river. The gradient variation of the river, the high slope in upstream with a sudden drop of gradient while entering the plains, causes heavy deposition in Manas river. Even though

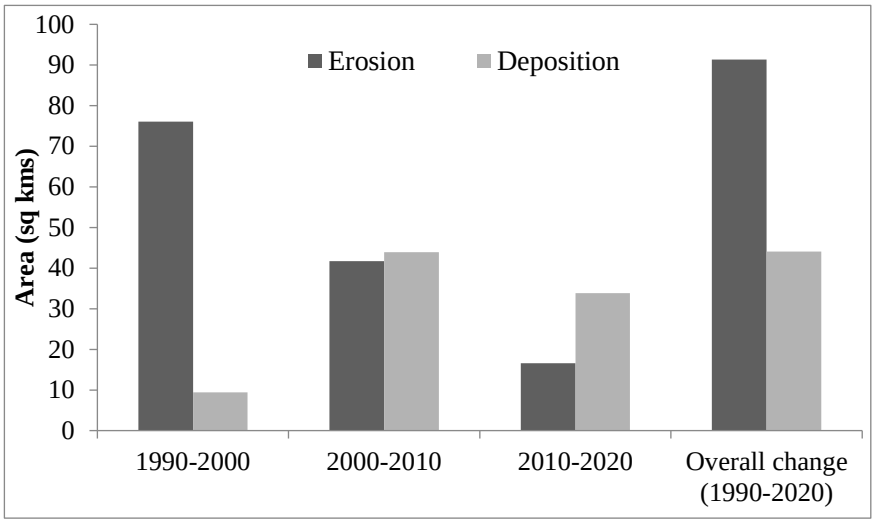

Figure 2.20 Erosion and deposition areas in Manas-Beki river during 1990-2020

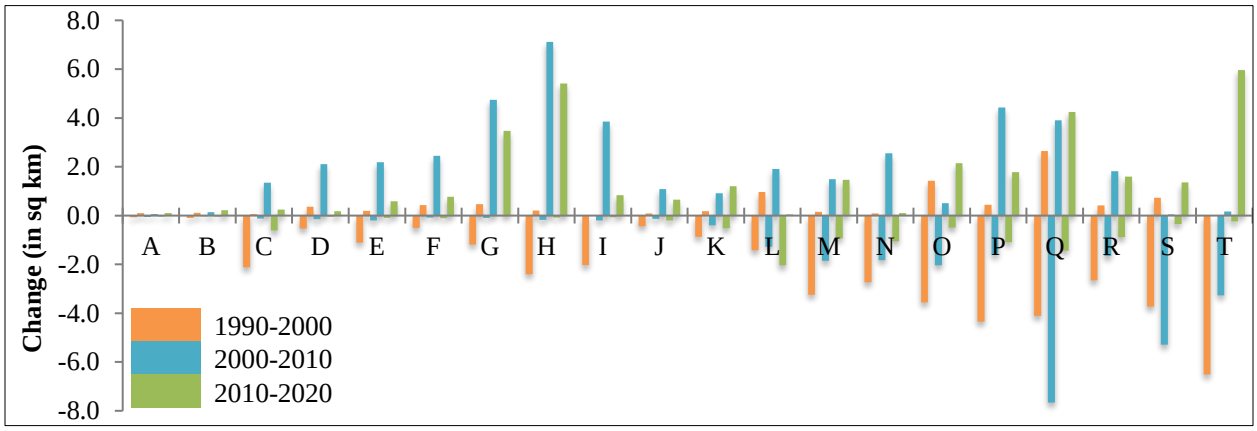

Figure 2.21(a) Erosion and deposition areas for each reach of Manas main channel *(negative values indicate erosion and positive values indicate deposition)*

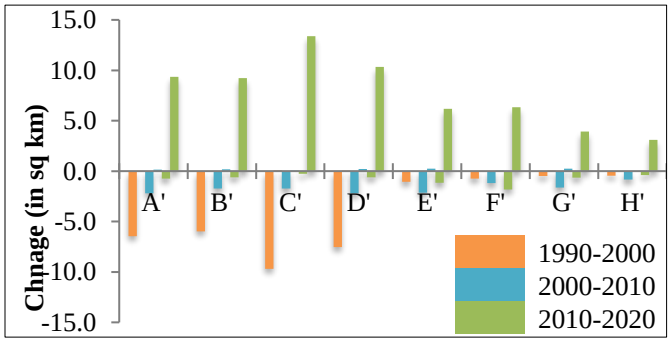

erosion areas are considerably exceeding deposition areas in the Manas-Beki river between 1990 to 2020, it is largely attributed to the high erosion during 1990-2000 during which period the major shift in thalweg occurred.

Figure 2.21(b) Erosion and deposition areas for each reach of Beki sub-section *(negative values indicate erosion and positive values indicate deposition)*

Table 2.11 Erosion and deposition areas for different reaches of Manas-Beki river during 1990-2020 (Areas in sq km)

Reach ID	1990-2000			2000-2010			2010-2020			Overall (1990-2020)		
	Erosion	Deposition	Net change	Erosion	Deposition	Net change	Erosion	Deposition	Net change	Erosion	Deposition	Net change
A	-0.07	0.09	0.02	-0.06	0.06	0.00	-0.04	0.10	0.06	-0.07	0.15	0.08
B	-0.10	0.12	0.02	-0.04	0.14	0.11	-0.04	0.22	0.17	-0.06	0.35	0.30
C	-2.11	0.06	-2.05	-0.12	1.35	1.24	-0.61	0.25	-0.36	-2.04	0.54	-1.50
D	-0.53	0.37	-0.17	-0.15	2.11	1.96	-0.04	0.18	0.14	-0.30	2.22	1.93
E	-1.11	0.20	-0.91	-0.21	2.19	1.99	-0.09	0.58	0.49	-0.57	2.14	1.56
F	-0.50	0.43	-0.07	-0.08	2.45	2.37	-0.10	0.77	0.67	-0.26	3.23	2.97
G	-1.18	0.46	-0.72	-0.10	4.75	4.65	-0.01	3.48	3.47	-0.15	7.56	7.40
H	-2.40	0.21	-2.19	-0.17	7.12	6.94	-0.08	5.41	5.33	-0.26	10.34	10.08
I	-2.03	0.02	-2.01	-0.20	3.86	3.65	-0.07	0.83	0.76	-0.22	2.64	2.41
J	-0.43	0.08	-0.35	-0.14	1.09	0.95	-0.20	0.66	0.45	-0.05	1.12	1.07
K	-0.87	0.17	-0.70	-0.40	0.92	0.52	-0.52	1.20	0.68	-1.18	1.68	0.50
L	-1.42	0.96	-0.46	-1.27	1.91	0.64	-2.04	0.04	-1.99	-2.53	0.71	-1.81
M	-3.25	0.15	-3.09	-1.85	1.49	-0.35	-0.93	1.47	0.54	-4.14	1.23	-2.91
N	-2.74	0.08	-2.65	-1.83	2.55	0.72	-1.05	0.11	-0.94	-4.44	1.56	-2.88
O	-3.55	1.43	-2.13	-2.03	0.51	-1.52	-0.48	2.14	1.66	-3.59	1.61	-1.98
P	-4.34	0.44	-3.90	-1.60	4.43	2.83	-1.10	1.78	0.68	-2.53	2.14	-0.39
Q	-4.11	2.65	-1.46	-7.66	3.91	-3.76	-1.43	4.24	2.81	-5.15	2.74	-2.41
R	-2.65	0.41	-2.24	-1.66	1.82	0.16	-0.88	1.59	0.71	-2.45	1.09	-1.37
S	-3.73	0.73	-3.00	-5.29	0.05	-5.24	-0.35	1.36	1.01	-8.01	0.79	-7.23
T	-6.50	0.00	-6.50	-3.27	0.16	-3.11	-0.24	5.96	5.72	-3.90	0.00	-3.90
A'	-6.44	0.03	-6.41	-2.19	0.19	-1.99	-0.74	0.06	-0.68	-8.76	0.00	-8.76
B'	-5.99	0.03	-5.96	-1.73	0.04	-1.69	-0.63	0.05	-0.57	-8.23	0.00	-8.22
C'	-9.69	0.08	-9.61	-1.71	0.20	-1.51	-0.28	0.22	-0.06	-11.20	0.02	-11.18
D'	-7.53	0.05	-7.48	-2.19	0.25	-1.94	-0.61	0.23	-0.38	-9.80	0.00	-9.80
E'	-1.07	0.03	-1.05	-2.13	0.06	-2.06	-1.16	0.33	-0.83	-4.01	0.07	-3.94
F'	-0.74	0.02	-0.72	-1.18	0.24	-0.94	-1.81	0.27	-1.55	-3.35	0.14	-3.21
G'	-0.50	0.06	-0.44	-1.62	0.02	-1.59	-0.65	0.26	-0.39	-2.43	0.00	-2.43
H'	-0.45	0.00	-0.45	-0.84	0.00	-0.84	-0.39	0.02	-0.37	-1.69	0.00	-1.68

Analysis of erosion and deposition for each reach shows that erosion occurred in almost all the reaches during 1990-2000. During 2000-2010, deposition was observed in almost all reaches of the Manas main channel except three reaches near the confluence region where large areas were eroded. In the Beki anabranch reach, erosion was observed but the areas were comparatively much smaller. During 2010-2020, large areas were deposited in both left and right bank anabranches above the NH crossing, as well as the reaches after the crossing. The change in confluence with the Brahmaputra over the years has also contributed to major changes in the region.

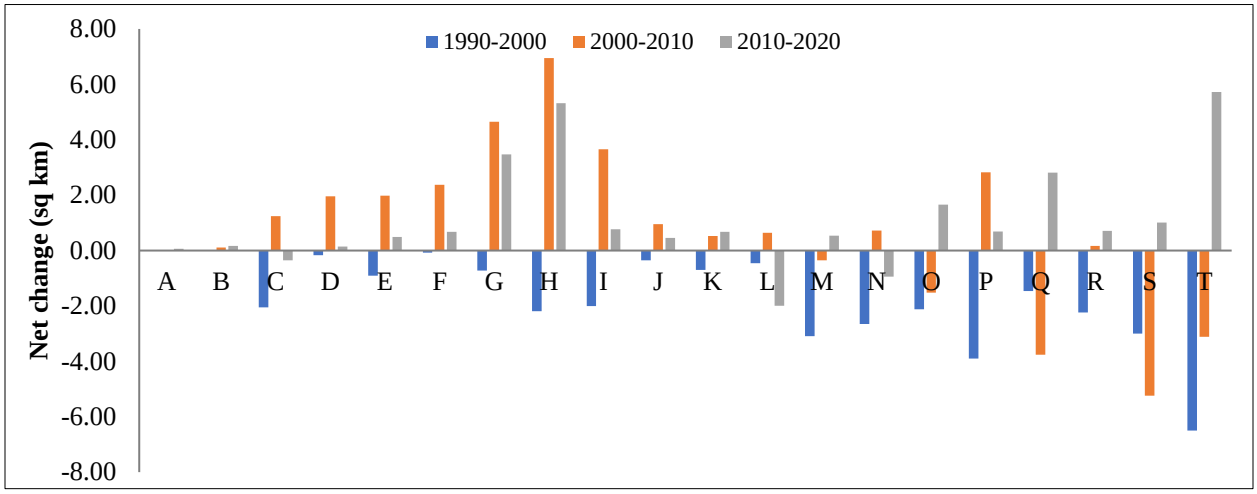

Figure 2.22(a) Net area change due to erosion and deposition for each reach of Manas main channel

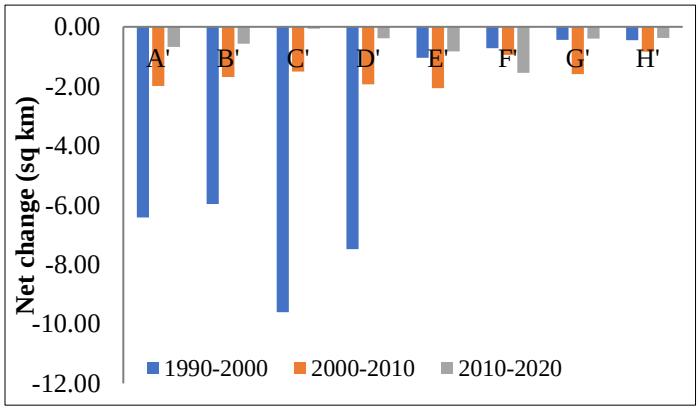

Figure 2.22(b) Net area change due to erosion and deposition for each reach of Beki sub-section

Values of net area change clearly show that erosion is the dominant process during 1990-2000 in almost all the reaches. Deposition was more than erosion in the right bank Manas anabranch section while erosion was dominant in the left bank Beki anabranch section during 2000-2010. Erosion was also the dominant process in the lower reaches before the Brahmaputra confluence. During 2010-2020, deposition was fairly dominant in the Manas anabranch as well as in the lower reaches after NH crossing, but erosion was still slightly dominant in the Beki anabranch section.

2.4 Discussion and summary

Morphometric analysis of the Manas-Beki river basin characterizes the basin as a highly dissected, moderately elongated basin with a steep descent in the Himalayan region and relatively flat topography in the floodplains. There is a sudden change in altitude between the Himalayan region and the Indian floodplains. All morphometric parameters are variable in the two distinct regions, but the overall characteristics are dominated by the high topography of the Himalayas. The hypsometry of the basin reveals the maximum area to be within the altitudes of 4500 to 5500 m a.m.s.l. More than 75% of the streams in the basin are characterized as first-order streams which together with the high range of altitude in the basin makes the basin highly sensitive to large runoff which is rapidly transported to the foothills [1]. Drainage density varies with slope and the catchment of Manas is largely spread in hilly areas, thus the number of streams is high and the mean stream length is low. The relatively low drainage density and flat slope of the floodplains is highly susceptible to changes in streamflow resulting in widespread flooding. The stream length ratio shows important relation with surface flow discharge and the erosion stage of a basin [69]. It does not vary largely for different order streams in the basin representing a young basin with high erosion potential. The bifurcation ratio of the basin is mostly in consistence with the Hortonian law of variation [56] and the values suggest low geologic control on drainage development. Relatively low values in the plains suggest a high probability of floods in the region [17]. The analysis of the areal and relief aspects of the basin suggests that the basin is subject to high overland flow with moderate water storage capacity. The high ultra-fine texture and high drainage density in the hills favours the rapid transport of runoff and sediments but the low slope and low drainage density in the plains indicate high chances of widespread flooding. The values are also suggestive of an active young basin where erosional processes are highly active and topographical maturity is not attained [70]. The morphometric analysis of the Manas-Beki river basin suggests that the basin would be sensitive to changes in streamflow, and downstream regions would be largely affected. This makes the basin highly susceptible to observed changes in the climate and further studies on the effect of climate change on the water availability of the basin are needed to understand the hydrological impacts.

Analysis of change during the last three decades shows that the most significant changes in the morphology of the Manas-Beki river system are in the flood plains and delineation of river thalweg and bank lines indicate immense changes in the channel. Analysis of the satellite images from

1990 to 2020 shows major visible changes in the flow paths of the Manas-Beki river in the floodplain region. The most significant change in river course between 1990 to 2020 is the gradual shifting of the main channel from the right bank Manas anabranch to the left bank Beki anabranch in the upper foothill region. This shift in the main channel of Manas led to abandonment of its only distributary to the Aie river flowing west of the Manas-Beki and thereby made Aie an independent river. The eventual shift of Manas to Beki has increased the flow discharge of the river. The aftermath can be seen in the change of planform geometry. The left bank Beki anabranch has formed more braiding. Beki which earlier had a lean flow now receives the entire discharge of Manas and Manas right anabranch has turned into a lean channel. The river has also changed its confluence point with the Brahmaputra frequently and even though the course is observed to be straightening, it flows parallel to the Brahmaputra for some time before draining into the Brahmaputra.

Anabranching is a common phenomenon and thalweg shift is prominent between anabranches over the years. The overall sinuosity of the river in the floodplain area is decreasing from 1990 to 2020. A slight decrease in the sinuosity indicates a gradual straightening over the years but the values remain less than 1.5 representing an immature river with high erosion potential. The sinuosity decreased considerably between 1990 and 2000 after which the decrease is very gradual. The floodplain reach of the river is observed to be braided in nature which shows that the river carries high sediment load and is associated with high gradient changes. The braiding nature also signifies the river has frequent variations in streamflow and weak bank material which is characteristic of the alluvial floodplain region. The analysis of braiding intensity in the floodplain region reveals that the braiding has highly increased in the left bank Beki anabranch and decreased in the right bank Manas anabranch. Downstream of the highway crossing, the braiding is intense, but no particular trend is noticed over the years.

The river thalwegs have shifted significantly during the last three decades. In 1990, the right bank Manas anabranch carried more discharge and the left bank Beki anabranch was a lean channel. This changed during 2000 when the left bank Beki anabranch was observed to be having higher discharge, Manas anabranch had lower flow pattern than the previous decade and the spatial pattern of flow was almost similar in both anabranches. In 2010 and 2020, the river completely shifted its major flow into the Beki anabranch and the Manas anabranch section turned into a lean

channel with minimal flow. Similar trends are observed in thalweg and bank line shifts during the years. Whereas the left bank is reasonably stable then the right bank for the Manas anabranch reach, which has shown a significant bank line migration, a significant change in bank lines has occurred in the Beki anabranch section due to the alteration of the direction of flow. Downstream of the NH crossing, the changes are highly erratic and do not have any specific trend. The confluence with the Brahmaputra is also observed to be changing over the years. The channel width shows an overall increase in the entire floodplain stretch of the river with only the right bank Manas anabranch reach showing a decrease, but this is minimal in comparison to the large increase in the Beki sub-section.

Erosion and deposition trends are also in line with the results of channel dynamics. Erosion is very high between 1990-2000 and decreases thereafter, while deposition increases. In the last decade, deposition areas have exceeded the erosion areas. Channel dynamics, erosion, and deposition trends in specific reaches indicate the influence of road and railway crossing and associated restricting constructions in this high-energy river system. The dynamics in channel morphology in the floodplain indicate high sediment influx into the floodplains from the Himalayan tributaries as observed by other researchers for the north bank tributaries of the Brahmaputra with their origin in the Himalayas [53, 46]. The reasons for this change in flow and sediment regime of the river need to be further investigated for possible links to the observed changes in climatic factors along with changes in the land cover of the basin.

2.5 References

[1] Patton, P.C. and Baker, V.R. Morphometry and floods in small drainage basins subject to diverse hydrogeomorphic controls. *Water Resources Research*, 12(5): 941-952, 1976. DOI: https://doi.org/10.1029/WR012i005p00941.

[2] Rosgen, D.L. A classification of natural rivers, *Catena*, 22: 169–199, 1994. DOI: https://doi.org/10.1016/0341-8162(94)90001-9.

[3] Lane, S.N., Tayefi, V., Reid, S.C., Yu, D. and Hardy, R.J. Interactions between sediment delivery, channel change, climate change and flood risk in a temperate upland environment. *Earth Surface Processes and Landforms*, 32: 429-446, 2007. DOI: https://doi.org/10.1002/esp.1404.

[4] Kiss, T. and Blanka, V. River channel response to climate- and human-induced hydrological changes: Case study on the meandering Hernád River, Hungary. *Geomorphology*, 175–176: 115-125, 2012. DOI: https://doi.org/10.1016/j.geomorph.2012.07.003.

[5] Singh, M., Sinha, R., and Tandon, S. K. Geomorphic connectivity and its application for understanding landscape complexities: a focus on the hydro-geomorphic systems of India. *Earth Surface Processes and Landforms*, 46(1): 110-130, 2021. DOI: https://doi.org/10.1002/esp.4945.

[6] Lord, M.L., Germanoski, D., and Allmendinger, N.E. Fluvial geomorphology: Monitoring stream systems in response to a changing environment. In Young, R. and Norby L., editors, *Geological Monitoring*, ISBN: 9780813760322, Geological Society of America, 2009. DOI: https://doi.org/10.1130/2009.monitoring(04).

[7] Ghosh, S., Islam, A., Das, P., Mukhopadhyay, A., Das Gupta, A., and Kumar Singh, A. Fluvial Systems in the Anthropocene: Important Concepts, Issues and Research Needs. In Islam, A., Das, P., Ghosh, S., Mukhopadhyay, A., Das Gupta, A., and Kumar Singh, A., editors, *Fluvial Systems in the Anthropocene*, pages 1-22, ISBN: 978-3-031-11180-8, Springer, Cham, 2022. DOI: https://doi.org/10.1007/978-3-031-11181-5_1.

[8] Horton, R.E. Drainage basin characteristics. *Transactions, American Geophysical Union*, 13(1):350-361, 1932.

[9] Gardiner, V. and Park, C. C. Drainage basin morphometry: review and assessment. *Progress in Physical Geography: Earth and Environment*, 2(1):1–35, 1978. DOI: https://doi.org/10.1177/030913337800200102.

[10] Reddy, G.P.O., Maji, A.K., and Gajbhiye, K.S. Drainage morphometry and its influence on landform characteristics in a basaltic terrain, Central India – a remote sensing and GIS approach. *International Journal of Applied Earth Observation and Geoinformation*, 6(1): 1-16, 2004. DOI: https://doi.org/10.1016/j.jag.2004.06.003.

[11] Bagyaraj, M. and Gurugnanam, B. Significance of Morphometry Studies, Soil Characteristics, Erosion Phenomena and Landform Processes Using Remote Sensing and GIS for Kodaikanal Hills, A Global Biodiversity Hotpot in Western Ghats, Dindigul District, Tamil Nadu, South India. *Research Journal of Environmental and Earth Sciences*, 3(3): 221-233, 2011.

[12] Ozdemir, H. and Bird, D. Evaluation of morphometric parameters of drainage networks derived from topographic maps and DEM in point of floods. *Environmental Geology*, 56:1405–1415, 2009. DOI: https://doi.org/10.1007/s00254-008-1235-y.

[13] Mahala, A. The significance of morphometric analysis to understand the hydrological and morphological characteristics in two different morpho-climatic settings. *Applied Water Science*, 10:33, 2020. DOI: https://doi.org/10.1007/s13201-019-1118-2.

[14] Pankaj, A. and Kumar, P. GIS-based morphometric analysis of five major sub-watersheds of Song River, Dehradun District, Uttarakhand with special reference to landslide incidences. *Journal of Indian Society of Remote Sensing*, 37:157–166, 2009. DOI: https://doi.org/10.1007/s12524-009-0007-9.

[15] Harlin, J.M. The effect of precipitation variability on drainage basin morphometry. *American Journal of Science*, 280:812-825, 1980.

[16] Tucker, G.E. and Slingerland, R. Drainage basin responses to climate change. *Water Resources Research*, 33(8): 2031-2047, 1997. DOI: https://doi.org/10.1029/97WR00409.

[17] Sah, R.K. and Das, A.K. Actualizing the role of morphometry in riverine hazards in an Eastern Himalayan river. *Arabian Journal of Geosciences*, 9:211, 2016. DOI: https://doi.org/10.1007/s12517-015-2144-5.

[18] Chaubey, P.K., Kundu, A., and Mall, R.K. A geo-spatial inter-relationship with drainage morphometry, landscapes and NDVI in the context of climate change: a case study over the Varuna river basin (India). *Spatial Information Research,* 27:627–641, 2019. DOI: https://doi.org/10.1007/s41324-019-00264-2.

[19] Alam, A., Ahmed, B., and Sammonds, P. Flash flood susceptibility assessment using the parameters of drainage basin morphometry in SE Bangladesh. *Quaternary International,* 575–576: 295-307, 2021. DOI: https://doi.org/10.1016/j.quaint.2020.04.047.

[20] Soille, P.J. and Ansoult, M.M. Automated basin delineation from digital elevation models using mathematical morphology, *Signal Processing,* 20(2): 171-182, 1990. DOI: https://doi.org/10.1016/0165-1684(90)90127-K.

[21] Marin, A-F. A methodological framework for the morphometric analysis of the fluvial islets along the Danube River in the Giurgiu – Oltenita sector. *GeoPatterns*, 1(2): 18-22, 2016.

[22] Biswas, S., Sudhakar, S., and Desai, V.R. Prioritisation of subwatersheds based on morphometric analysis of drainage basin: a remote sensing and gis approach. *Journal of the Indian Society of Remote Sensing*, 27:155–166, 1999. DOI: https://doi.org/10.1007/BF02991569.

[23] Mesa, L.M. Morphometric analysis of a subtropical Andean basin (Tucumán, Argentina). *Environmental Geology,* 50:1235–1242, 2006. DOI: https://doi.org/10.1007/s00254-006-0297-y.

[24] Rudraiah, M., Govindaiah, S., and Vittala, S.S. Morphometry using remote sensing and GIS techniques in the sub-basins of Kagna river basin, Gulburga district, Karnataka, India *Journal of the Indian Society of Remote Sensing*, 36:351–360, 2008. DOI: https://doi.org/10.1007/s12524-008-0035-x.

[25] Magesh, N.S., Jitheshlal, K.V., Chandrasekar, N., and Jini, K.V. Geographical information system-based morphometric analysis of Bharathapuzha river basin, Kerala, India. *Applied Water Science,* 3:467–477, 2013. DOI: https://doi.org/10.1007/s13201-013-0095-0.

[26] Pande, C.B. and Moharir, K. GIS based quantitative morphometric analysis and its consequences: a case study from Shanur River Basin, Maharashtra India. *Applied Water Science*, 7:861–871, 2017. DOI: https://doi.org/10.1007/s13201-015-0298-7.

[27] Manjare, B.S., Reddy, G.P.O. & Kamble, S. Evaluation of basin morphometric indices and tectonic implications in sedimentary landscape, Central India: A remote sensing and GIS approach. *Environmental Earth Science*, 80:659, 2021. DOI: https://doi.org/10.1007/s12665-021-09947-2.

[28] Gurnell, A. M., Downward, S. R., and Jones, R. Channel planform change on the river dee meanders, 1876–1992. *River Research and Applications*, 9(4): 187-204, 1994. DOI: https://doi.org/10.1002/rrr.3450090402.

[29] Goswami, U., Sarma, J.N. and Patgiri, A.D. River channel changes of the Subansiri in Assam, India. *Geomorphology*, 30: 227-244, 1999. DOI: https://doi.org/10.1016/S0169-555X(99)00032-X.

[30] Schumm, S. A. Patterns of alluvial rivers. *Annual Review of Earth and Planetary Sciences*, 13(1):5-27, 1985. DOI: https://doi.org/10.1146/annurev.ea.13.050185.000253.

[31] Huang, J. and Ma, G. Application of remote sensing and GIS to the assessment of bank stability in the Lower Yangtze River, In *SPIE Optical Remote Sensing for Industry and Environmental Monitoring*, Volume 3504, Beijing, China, 1998. DOI: https://doi.org/10.1117/12.319538.

[32] Laliberte, A.S., Johnson, Harris, D.E., Harris, N.R., and Casady, G.R. Stream change analysis using remote sensing and Geographic Information Systems (GIS). *Journal of Range Management*, 54(2): A22-A50, 2001. DOI: https://doi.org/10.2307/4003189.

[33] Boruah, S., Gilvear, D., Hunter, P., and Sharma, N. Quantifying channel planform and physical habitat dynamics on a large braided river using satellite data—the Brahmaputra, India. *River Research and Applications*, 24(5): 650-660, 2008. DOI: https://doi.org/10.1002/rra.1132.

[34] Rudra, K. Dynamics of the Ganga in West Bengal, India (1764–2007): Implications for science–policy interaction. *Quaternary International*, 227(2):161-169, 2010. DOI: https://doi.org/10.1016/j.quaint.2009.10.043.

[35] Sinha, R. and Ghosh, S. Understanding dynamics of large rivers aided by satellite remote sensing: a case study from Lower Ganga plains, India, *Geocarto International*, 27(3):207-219, 2012. DOI: https://doi.org/10.1080/10106049.2011.620180.

[36] Bhuiyan, M.A.H., Kumamoto, T., and Suzuki, S. Application of remote sensing and GIS for evaluation of the recent morphological characteristics of the lower Brahmaputra-Jamuna River, Bangladesh. *Earth Science Informatics*, 8:551–568, 2015. DOI: https://doi.org/10.1007/s12145-014-0180-4.

[37] Langat, P.K., Kumar, L., and Koech, R. Monitoring river channel dynamics using remote sensing and GIS techniques. *Geomorphology,* 325: 92-102, 2019. DOI: https://doi.org/10.1016/j.geomorph.2018.10.007.

[38] Rahman, M.R. River dynamics – a geospatial analysis of Jamuna (Brahmaputra) River in Bangladesh during 1973–2019 using Landsat satellite remote sensing data and GIS. *Environmental Monitoring and Assessment*, 195:96, 2023. DOI: https://doi.org/10.1007/s10661-022-10638-z.

[39] Das, A.K., Sah, R.K., and Hazarika, N. Bankline change and the facets of riverine hazards in the floodplain of Subansiri–Ranganadi *Doab*, Brahmaputra Valley, India. *Natural Hazards*, 64:1015–1028, 2012. DOI: https://doi.org/10.1007/s11069-012-0283-5.

[40] Ortega, J. A., Razola, L., and Garzón, G. Recent human impacts and change in dynamics and morphology of ephemeral rivers. *Natural Hazards and Earth System Sciences,* 14:713–730, 2014. DOI: https://doi.org/10.5194/nhess-14-713-2014.

[41] Rinaldi, M., Surian, N., Comiti, F., and Bussettini, M. A methodological framework for hydromorphological assessment, analysis and monitoring (IDRAIM) aimed at promoting integrated river management. *Geomorphology,* 251: 122-136, 2015. DOI: https://doi.org/10.1016/j.geomorph.2015.05.010.

[42] Saleem, A., Dewan, A., Rahman, M.M., Nawfee, S.M., Karim, R., and Lu, X.X. Spatial and Temporal Variations of Erosion and Accretion: A Case of a Large Tropical River. *Earth Systems and Environment*, 4:167–181, 2020. DOI: https://doi.org/10.1007/s41748-019-00143-8.

[43] Langat, P.K., Kumar, L., Koech, R., and Ghosh, M.K. Characterisation of channel morphological pattern changes and flood corridor dynamics of the tropical Tana River fluvial systems, Kenya. *Journal of African Earth Sciences,* 163: 103748, 2020. DOI: https://doi.org/10.1016/j.jafrearsci.2019.103748.

[44] Boothroyd, R.J., Nones, M., and Guerrero, M. Deriving Planform Morphology and Vegetation Coverage From Remote Sensing to Support River Management Applications. *Frontiers in Environmental Science*, 9, 2021. DOI: https://doi.org/10.3389/fenvs.2021.657354.

[45] Zhang, Q., Hu, K., Wei, L., and Liu, W. Rapid changes in fluvial morphology in response to the high-energy Yigong outburst flood in 2000: Integrating channel dynamics and flood hydraulics. *Journal of Hydrology*, 612(B): 128199, 2022. DOI: https://doi.org/10.1016/j.jhydrol.2022.128199.

[46] Sah, R.K., Kumar, D.N., and Das, A.K. Channel evolution of the Himalayan tributaries in northern Brahmaputra plain in recent centuries. *Acta Geophysica*, 70:1317–1330, 2022. DOI: https://doi.org/10.1007/s11600-022-00780-0.

[47] Morais, E.S., Rocha, P.C., and Hooke, J. Spatiotemporal variations in channel changes caused by cumulative factors in a meandering river: The lower Peixe River, Brazil. *Geomorphology*, 273:348-360, 2016. DOI: https://doi.org/10.1016/j.geomorph.2016.07.026.

[48] Ulloa, H., Mazzorana, B., Batalla, R.J., Jullian, C., Iribarren-Anacona, P., Barrientos, G., Reid, B., Oyarzun, C., Schaefer, M., and Iroumé, A. Morphological characterization of a highly-dynamic fluvial landscape: The River Baker (Chilean Patagonia). *Journal of South American Earth Sciences*, 86: 1-14, 2018. DOI: https://doi.org/10.1016/j.jsames.2018.06.002.

[49] Roccati, A., Faccini, F., Luino, F., De Graff, J.V., and Turconi, L. Morphological changes and human impact in the Entella River floodplain (Northern Italy) from the 17th century. *Catena*, 182: 104122, 2019. DOI: https://doi.org/10.1016/j.catena.2019.104122.

[50] East, A.E. and Sankey, J.B. Geomorphic and Sedimentary Effects of Modern Climate Change: Current and Anticipated Future Conditions in the Western United States. *Reviews of Geophysics*, 58(4): e2019RG000692, 2020. DOI: https://doi.org/10.1029/2019RG000692.

[51] Shit, P.K., Bera, B., Islam, A., Ghosh, S., and Bhunia, G.S. Introduction to Drainage Basin Dynamics: Morphology, Landscape and Modelling. In Shit, P.K., Bera, B., Islam, A., Ghosh, S., and Bhunia, G.S., editors, *Drainage Basin Dynamics. Geography of the Physical Environment*, pages 1-9, ISBN: 978-3-030-79633-4, Springer, Cham, 2022. DOI: https://doi.org/10.1007/978-3-030-79634-1_1.

[52] Kayitesi, N.M., Guzha, A.C., and Mariethoz, G. Impacts of land use land cover change and climate change on river hydro-morphology- a review of research studies in tropical regions. *Journal of Hydrology*, 615(A): 128702, 2022 DOI: https://doi.org/10.1016/j.jhydrol.2022.128702.

[53] Sah, R.K. and Das, A.K. Morphological Dynamics of the Rivers of Brahmaputra. *Journal of the Geological Society of India*, 92:441-448, 2018. DOI: https://doi.org/10.1007/s12594-018-1039-y.

[54] Strahler, A.N. Quantitative geomorphology of drainage basin and channel networks. In Chow, V.T., editor, *Handbook of applied hydrology*, McGraw Hill Book Co, New York, pages 439–476, 1964.

[55] Sah, R. K. and Das, A. K. Minimizing ambiguities in stream classification of complex drainage structures. *Journal of Hydrology*, 553:224-230, 2017. DOI: https://doi.org/10.1016/j.jhydrol.2017.07.047.

[56] Horton, R.E. Erosional development of streams and their drainage basins; hydro physical approach to quantitative morphology. *Geological Society of America Bulletin*, 56(3):275-370, 1945. DOI: https://doi.org/10.1130/0016-7606(1945)56[275:EDOSAT]2.0.CO;2.

[57] Smith, K. G. Standards for grading texture of erosional topography. *American Journal of Science*, 248(9):655-668, 1950. DOI: https://doi.org/10.2475/ajs.248.9.655.

[58] Schumm, S.A. Evolution of drainage systems and slopes in Badlands at Perth Amboy, New Jersey. *Geological Society of America Bulletin*, 67(5):597-646, 1956. DOI: https://doi.org/10.1130/0016-7606(1956)67[597:EODSAS]2.0.CO;2.

[59] Miller, V.C. A Quantitative geomorphic study of drainage basin characteristic in the Clinch Mountain area, Virginia and Tennessee. Technical Report 3, Proj. NR 389-402, Department of Geology, Columbia University, ONR, New York, 1953.

[60] Schumm, S.A. Sinuosity of alluvial rivers on the great plains. *Geological Society of America Bulletin*, 74(9):1089-1100, 1963. DOI: https://doi.org/10.1130/0016-7606(1963)74[1089:SOAROT]2.0.CO;2.

[61] Friend, P.F. and Sinha, R. Braiding and meandering parameters. In Best, J.L. and Bristow, C.S., editors, *Braided Rivers*, pages 105–112, The Geological Society, London, 1993.

[62] Howard, A.D., Keetch, M.E., and Vincent, C.L. Topological and geometrical properties of braided streams. *Water Resources Research*, 6: 1674-1688, 1970. DOI: https://doi.org/10.1029/WR006i006p01674.

[63] Strahler, A.N. Quantitative analysis of watershed geomorphology. *Transactions, American Geophysical Union,* 38(6):913-920, 1957.

[64] Mangesh, N.S., Chandrasekar, N., and Soundranayagam, J.P. Morphometric evaluation of Papanasam and Manimuthar watersheds, parts of Western Ghats, Tirunelveli district, Tamil Nadu, India: a GIS approach. *Environmental Earth Sciences*, 64(2):373-381, 2011. DOI: https://doi.org/10.1007/s12665-010-0860-4.

[65] Ramakrishnan, D., Bandyopadhyay, A., and Kusuma, K.N. SCS-CN and GIS-based approach for identifying potential water harvesting sites in the Kali watershed, Mahi River basin, India. *Journal of Earth System Science,* 118(4):355-368, 2009.

[66] Melton, M. A. Correlation structure of morphometric properties of drainage systems and their controlling agents. *The Journal of Geology,* 66(4):442-460, 1958.

[67] Strahler, A.N. Dimensional analysis applied to fluvially eroded landforms. *Geological Society of America Bulletin*, 69(3):279-300, 1958.

[68] Egozi, R. and Ashmore, P. Defining and measuring braiding intensity. *Earth Surface Processes and Landforms,* 33:2121-2138, 2008. DOI: https://doi.org/10.1002/esp.1658.

[69] Zaidi, F.K. Drainage basin morphometry for identifying zones for artificial recharge: a case study from the Gagas River basin, India. *Journal Geological Society of India*, 77(2):160-166, 2011.

[70] Rai, P.K., Mohan, K., Mishra, S., Ahmad, A., and Mishra, V.N. A GIS-based approach in drainage morphometric analysis of Kanhar River Basin, India. *Applied Water Science,* 7:217–232, 2017. DOI: https://doi.org/10.1007/s13201-014-0238-y.